SMALL DISTURBANCE THEORY FOR HYPERSONIC FLOW OVER SLENDER BODIES

by

ANDREW WILLIAM WUETCHER

XIAOWEN WANG, COMMITTEE CHAIR
GARY CHENG
TIMOTHY JORRIS
SEMIH M. OLCMEN

A THESIS

Submitted in partial fulfillment of the requirements
for the degree of Master of Science
in the Department of Aerospace Engineering and Mechanics
in the Graduate School of
The University of Alabama

TUSCALOOSA, ALABAMA

2019

ABSTRACT

Hypersonic flows involve high-enthalpy free-stream conditions. As a result, high temperature effects, which include internal energy excitations, energy relaxations, and chemical reactions, become important. Taking into account these high temperature effects makes it difficult and time consuming to calculate the flow field of a hypersonic flow. Fortunately, for the preliminary/conceptual design of hypersonic vehicles that are generally slender bodies, one can neglect the transport terms (mass, momentum, and energy). Hence, an approximate self-similar solution of the hypersonic flow field might be obtained by solving the inviscid governing equations. The goal of this research is to develop a reliable and efficient tool that drastically reduces the computational time for the approximate calculation of a hypersonic flow field using hypersonic small disturbance theory. A MATLAB code has been developed and tested that is capable of calculating hypersonic flows under perfect gas and diatomic dissociating gas approximations. Hypersonic flows on a circular cone, a plane wedge, and power-law shock bodies are firstly calculated based on perfect gas approximations. Flow characteristics of the cone and wedge results agree well with the oblique shock theory solutions. Hypersonic flows on power-law shock bodies are then calculated based on diatomic dissociating gas approximations. The results agree well with those in the literature. These calculations for the perfect gas and diatomic dissociating gas models shed light on the further development of small disturbance theory for more complex hypersonic flows.

DEDICATION

This thesis is dedicated to my mother and grandfather.

LIST OF ABBREVIATIONS AND SYMBOLS

b	Ratio of body angle to shock-wave angle
B	Body surface
C_p	Coefficient of pressure
$c_{v,s}$	Species translation-rotation heat capacity at constant volume
D	Dissociation energy per molecule
E	Energy
e	Specific total energy
e_v	Species vibration energy
$e_{v,s}$	Species specific vibration energy
F_j	Inviscid flux vector
G_j	Viscous flux vector
h	Enthalpy
h_s°	Species heat of formation
$HSDT$	Hypersonic small disturbance theory
k	Boltzmann's constant
K	Similarity parameter
k_T	Translation-rotation thermal conductivity
k_V	Vibration thermal conductivity
m	Body coefficient
M	Mach
M_s	Species Molecular Weight
ns	Number of species

p	Pressure
Q_{T-V_s}	Species vibration energy transfer rate
r	Carteisan coordinate y for plane flow
RMS	Root Mean Square
s	Entropy
S	Shock surface
X_r	Molar concentration of species r
T	Temperature
T_V	Vibrational Temperature
T_a	Defining temperature for the reaction
U	State Vector of Conservative Quantities
u_j	Velocity in jth direction
v	Velocity component in r direction
v_{ij}	Species diffusion velocity
W	Source vector
Subscripts	
b	body
c	characteristic
C	Cone
s	species
w	wave
∞	Freestream
Greek Symbols	
α	Degree of dissociation
β	$\sqrt{M^2-1}$
γ	Specific heat ratio
δ	Body angle

δ_{ij}	Kronecker delta
θ	Shock angle
$\theta_{v,s}$	Characteristic temperature of each vibrational model
μ	Viscosity
ρ	Density
ρ_s	Species density
ρ_c	Characteristic density
τ	$\frac{\delta}{b}$
τ_{ij}	Viscous stress
ψ	Stream function
ω	Normalized density

Functions

$f(z)$	Pressure function
$\chi(z)$	Arbitrary function
$\phi(z)$	Velocity function
$\psi(z)$	Density function

ACKNOWLEDGMENTS

I would like to thank my advisor, Dr. Xiaowen Wang for his incredible knowledge, guidance and support throughout this research project. I would also like to thank my committee members, Dr. Gary Cheng, Dr. Timothy Jorris and Dr. Semih Olcmen for their support of this dissertation and my academic progress. I would like to thank Dr. John Baker, Dr. Richard Branam and Dr. Paul Hubner for their support throughout my academic career. I would also like to thank my friends, John Kennamer, Hunter Goens and Christopher Simpson for their support during my graduate school career.

CONTENTS

LIST OF TABLES

LIST OF FIGURES

CHAPTER 1

INTRODUCTION

Hypersonic flows involve high-enthalpy free-stream conditions. As a result, high temperature effects, which include internal energy excitations, energy relaxations, and chemical reactions, become important. Taking into account these high temperature effects makes it difficult and time consuming to calculate a hypersonic flow field. Fortunately, current and future hypersonic vehicles (see Figs. 1.1 and 1.2) are generally slender bodies, which makes it possible to develop efficient methods for the approximate calculation of hypersonic flow fields.

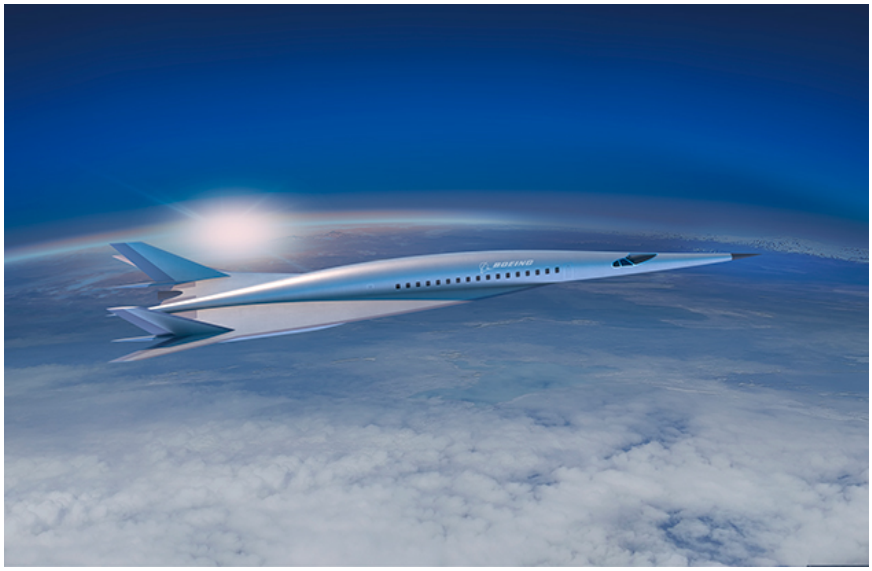

Figure 1.1: The first passenger-carrying hypersonic vehicle concept of Boeing [1]

In previous studies, small disturbance theory has been used to analyze incompressible, subsonic, transonic, and supersonic flows. This approach was applied to hypersonic flow

[1] https://www.boeing.com/features/2018/06/hypersonic-concept-vehicle.page

(a) Hypersonic Technology Vehicle 2 (HTV2)[2]

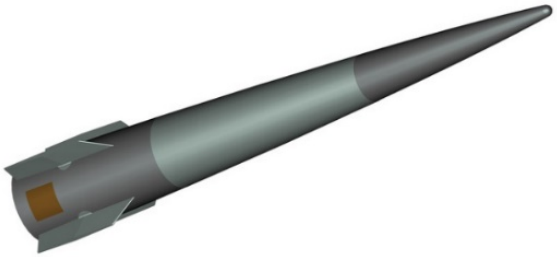

(b) Hyper Velocity Projectile[3]

Figure 1.2: Defense Related Hypersonic Vehicles

by van Dyke [1] for perfect gas flow. In his research, he concluded that by neglecting the viscosity, the velocity disturbances of the flow field would remain small. That is to say, the analysis shifts from using the freestream velocity as the dependent variable to instead using the change in velocity relative to the freestream. After van Dykes pioneering work, hypersonic small disturbance theory (HSDT) has since been used to approximate flow field characteristics around several different geometric bodies.

As a geometric body approaches a high Mach number, the linear aspect of the flow field breaks down and the flow field becomes nonlinear [1]. Because of this breakdown, the hypersonic similarity rule that was developed by Tsien and Hayes [2, 3] was required to apply small disturbance theory to hypersonic flow. Tsien used the same methodology that von Karman used for transonic flow. Essentially, he reduced the differential equations for hypersonic flow to a single non-dimensional equation [2]. In his research, Tsien found that if a series of bodies having the same distribution thickness but different thickness ratios,$(\frac{\delta}{b})$,where δ is the body angle and b is the ratio of the body angle to the shock-wave angle, were placed into flows of different Mach numbers, they would exhibit similar flow characteristics [2]. This thickness ratio is illustrated by Fig. 1.3. This flow similarity was valid, if the product of the freestream Mach, M, and the thickness ratio remained constant

[2]https://www.darpa.mil/about-us/timeline/falcon-htv-2

[3]https://www.baesystems.com/en-us/product/hyper-velocity-projectile-hvp

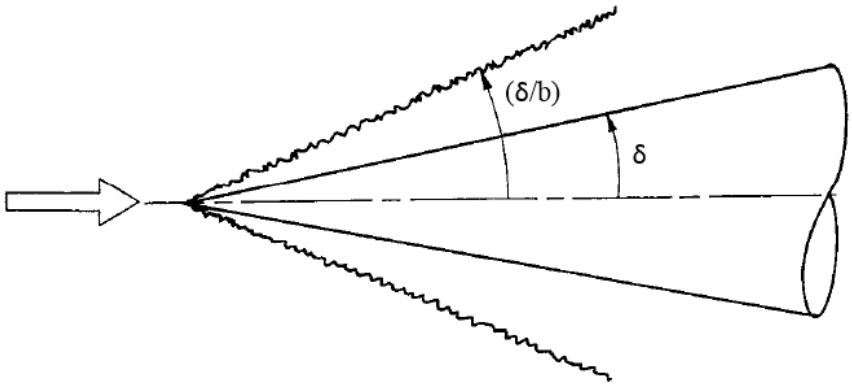

Figure 1.3: Thickness Ratio on a Circular Cone

and was equal to a similarity parameter, K. This relationship is shown in equation (1.1).

$$K = M(\frac{\delta}{b}) = M\tau \tag{1.1}$$

In his analysis, Tsien limited the usage of this similarity parameter to irrotational flow and axially symmetric geometric shapes [2]. This was improved upon by Hayes in his research that expanded the usage of the hypersonic similarity parameter to rotational flow and three-dimensional geometric shapes [3]. Follow on research by Hamaker and Wong [4] would add unsteady motion. Overall, hypersonic similarity was applicable to irrotational or rotational flow, axially symmetric or three-dimensional geometric shapes and to unsteady motion. This hypersonic similarity parameter laid the underlying theoretical foundation for the HSDT that van Dyke would obtain in his research.

In his development of HSDT, van Dyke [1] made several assumptions. The first is that viscosity and heat are neglected, thus allowing for the flow field to be approximated by small disturbance theory. The second is that the body is thin and is measured by the thickness ratio, $(\frac{\delta}{b})$ also known as τ. The third assumption is that the freestream Mach number is hypersonic. With the third assumption, linearized theory is unable to predict the flow field. Thus a criteria for hypersonic small disturbance theory could be established

and is shown in equation (1.2).

$$\left.\begin{array}{l}\tau \ll 1 \\ M \gg 1\end{array}\right\} with\ M\tau \sim 1\ or \gg 1 \tag{1.2}$$

Using these assumptions and criteria, van Dyke would establish the overall HSDT for perfect gas flow before modifying it for several different geometric bodies.

Following the overall development of HSDT, van Dyke [1, 5] applied the theory to several examples and compared theoretical and experimental results when available. In the first comparable example, a plane wedge was examined. This comparison showed that the results compared well at higher Mach numbers, however at lower Mach numbers the results deviated. To further improve HSDT at lower Mach numbers, unified supersonic-hypersonic theory was applied. With this correction, HSDT was able to be used not only for hypersonic Mach numbers but also supersonic Mach numbers. In the second comparable example, HSDT was applied to the initial gradients for a plane ogive. In the results it could be seen that van Dykes approximations were comparable to the approximate results that were developed by Kraus [6] in his research of supersonic flow at the leading edge of a curved airfoil. In further examples, van Dyke applied HSDT to a circular cone and the initial gradients on an ogive of revolution and compared it to the approximate solutions. For van Dyke's research, perfect gas flow, $\gamma = 1.405$, was used in all approximation cases. The HSDT developed by van Dyke was replicated and validated by Anderson [7] and Truitt [8] in their own work.

Further analysis of HSDT applied to a circular cone was conducted by Rasmussen [9] . In his study of hypersonic flow over an unyawed circular cone, Rasmussen was able to obtain the shock angle and surface pressure. The surface pressure in the form of the (C_{pb}/δ^2) was found to be 2.091 which compared to van Dykes pressure of 2.094. In follow on research, Doty and Rasmussen [10] applied HSDT to an inclined circular cone. In their research, they derived an approximate solution using small perturbation theory and found

that this solution could provide an answer that was in good agreement with previously developed approximate solutions. Furthermore, Moulder and D′Souza [11] developed HSDT for a conical axisymmetric flow behind an inverted shock and an axisymmetric Busemann shock. They concluded that when HSDT was applied to internal flows,the similarity laws developed by Tsien were required. Additionally, HSDT can be used to find flow parameters of internal flows as long as the assumptions set by van Dyke [1] are not violated.

Further development of HSDT was carried out by Kubota [12] to a slender blunt-nosed / power-law shock body in which he compared theoretical and experimental results. In his research, Kubota assumed the conditions at the shock wave (velocity, pressure and density) were known and integrated towards the body. The surface of the body was found when the velocity function became equal to the integrating factor. From his analysis, Kubota concluded that his solution compared well with that of Coles Newtonian Flow Theory [13] when the slender blunt-nosed body coefficient, m, was close to unity. But this result degraded as it approached a value of $m = 1/2$. Furthermore, in his experimental investigation, Kubota found that his theoretical results agreed with his experimental results once a boundary layer correction was applied to the theoretical results.

Following the work of Kubota, Meyer [14] extended the results of a slender blunt-nosed body for perfect gas to that for a diatomic dissociating gas. This enabled the gas to be characterized by a thermodynamically consistent equation of state. The approximation was valid over a range of dissociations and densities, including Lighthills [15] ideal dissociating gas. Meyers work closely follows the work of van Dyke by establishing the same variables and equations of motion of HSDT for a diatomic dissociating gas. Like Kubota, Meyer used the same geometric coordinates and began his evaluation of the flow field by starting at the shock and integrating towards the surface of the body. In the comparison of a perfect gas to a dissociating gas, a slender blunt-nosed body with coefficient, $m = 1$ and $1/2$, were used. The results for the dissociating gas approached the perfect gas results as the freestream density increased. This was to be expected since the degree of dissocia-

tion decreases with an increasing freestream density. Meyer concluded that the results of a dissociating gas agreed qualitatively but not quantitatively with Kubotas results for a perfect gas.

Previous research has primarily focused on the application of HSDT to circular cone type geometric bodies in a perfect gas flow. As the Mach number increases, hypersonic flows involve high-enthalpy freestream conditions. As a result, high temperature effects become important. Fortunately, for the preliminary design of hypersonic vehicles, one can neglect the transport terms (mass, momentum, and energy). Hence, an approximate solution of flow field can be obtained by solving the inviscid governing equations. The goal of this research is to develop a reliable and efficient tool for the approximate calculation of hypersonic flow field using hypersonic small disturbance theory. Hypersonic flows on a circular cone, a plane wedge, and power-law shock bodies are firstly calculated based on perfect gas approximations. Hypersonic flows on power-law shock bodies are then calculated based on diatomic dissociating gas approximations.

CHAPTER 2

GOVERNING EQUATIONS OF HSDT FOR GENERAL HYPERSONIC FLOW

As an example of general hypersonic flow, a five-species gas model composed of N_2, O_2, NO, N, and O is used for air. This model will be valid for air temperature below 9000 $^{\circ}K$. Based on a two-temperature model for internal energy [16], the governing equations are the three-dimensional Navier-Stokes equations which consist of five mass conservation equations, three momentum conservation equations, the vibrational energy conservation equation, and the global energy conservation equation. The governing equation in vector form is defined in equation (2.1).

$$\frac{\partial U}{\partial t} + \frac{\partial F_j}{\partial x_j} + \frac{\partial G_j}{\partial x_j} = W \tag{2.1}$$

Where U is the state vector of conservative quantities and source term W is defined in equation (2.2)

$$U = \begin{bmatrix} \rho_{N_2} \\ \rho_{O_2} \\ \rho_{NO} \\ \rho_N \\ \rho_O \\ \rho u_1 \\ \rho u_2 \\ \rho u_3 \\ \rho e \\ \rho e_v \end{bmatrix} \quad W = \begin{bmatrix} W_{N_2} \\ W_{O_2} \\ W_{NO} \\ W_N \\ W_O \\ 0 \\ 0 \\ 0 \\ 0 \\ \sum_{s=1}^{nms} \left(Q_{T-V,s} + W_s e_{v,s} \right) \end{bmatrix} \tag{2.2}$$

where e_v is the specific vibration energy, $Q_{T-V,s}$ is the species vibration energy transfer rate and $e_{v,s}$ is the species specific vibration energy. The flux is split into its inviscid, convective components, F_j, and viscous, diffusive components, G_j, as defined in equation (2.3)

$$F_j = \begin{bmatrix} \rho_{N_2} u_j \\ \rho_{O_2} u_j \\ \rho_{NO} u_j \\ \rho_N u_j \\ \rho_O u_j \\ \rho u_1 u_j + p\delta_{1j} \\ \rho u_2 u_j + p\delta_{2j} \\ \rho u_3 u_j + p\delta_{3j} \\ (\rho e + p)\, u_j \\ \rho e_v u_j \end{bmatrix} \quad G_j = \begin{bmatrix} \rho_{N_2} v_{N_{2j}} \\ \rho_{O_2} v_{O_{2j}} \\ \rho_{NO} v_{NO_j} \\ \rho_N v_{N_j} \\ \rho_O v_{O_j} \\ \tau_{j1} \\ \tau_{j2} \\ \tau_{j3} \\ -\tau_{ji} u_j - k_T \frac{\partial T}{\partial x_j} - k_v \frac{\partial T_V}{\partial x_j} + \sum_{s=1}^{nms} \rho_s h_s v_{sj} \\ -k_v \frac{\partial T_V}{\partial x_j} + \sum_{s=1}^{nms} \rho_s h_s v_{sj} \end{bmatrix} \tag{2.3}$$

where δ_{ij} is the Kronecker delta, v_{sj} is the species diffusion velocity,τ_{ij} is the viscous stress, k_T is the translation-rotation thermal conductivity, and k_v is vibration thermal conductiv-

ity. The total energy per unit volume, ρe, is defined by equation (2.4),

$$\rho e = \sum_{s=1}^{nms} \rho_s c_{v,s} T + \rho e_v + \frac{1}{2}\rho u_i u_i + \sum_{s=1}^{ns} \rho_s h_s^{\circ} \tag{2.4}$$

where h_s° is the heat of formation of the species s, nms is the number of molecular species, ns is the number of species and $c_{v,s}$ is the species translation-rotation specific heat at constant volume defined in equation (2.5).

$$c_{v,s} = \begin{cases} \frac{5}{3}\frac{R}{M_s}, & s = 1, 2, \ldots, nms \\ \frac{3}{2}\frac{R}{M_s}, & s = nms+1, \ldots, ns. \end{cases} \tag{2.5}$$

The vibration energy per unit volume, ρe_v, is defined as equation (2.6)

$$\rho e_v = \sum_{s=1}^{nms} \rho_s e_{v,s} = \sum_{s=1}^{nms} \rho_s \frac{R}{M_s} \frac{\theta_{v,s}}{\exp(\theta_{v,s}/T_V) - 1} \tag{2.6}$$

where M_s is the species molecular weight, $\theta_{v,s}$ refers to the characteristic temperature of each vibrational model and T_V is the vibrational temperature. The characteristic vibration temperatures are taken from Park [17]. The values of h_s°, M_s and $\theta_{v,s}$ are shown in Table 2.1.

Table 2.1: Values of h_s°, M_s and $\theta_{v,s}$

Species	h_s° (J/kg)	M_s (g)	$\theta_{v,s}$ (K)
N_2	0	28	3395
O_2	0	32	2239
NO	2.996123e6	30	2817
N	3.362161e7	14	-
O	1.543119e7	16	-

The chemical model for a five species air has three dissociation reactions and three

exchange reactions, as defined by Mortenson [18]. The dissociation reactions take the form of equation (2.7)

$$R_c = \sum_{s=1}^{ns} \left(-k_{f,c,s} \frac{\rho_r}{M_r} \frac{\rho_s}{M_s} + k_{b,c,s} \frac{\rho_{p1}}{M_{p1}} \frac{\rho_{p2}}{M_{p2}} \frac{\rho_s}{M_s} \right) \tag{2.7}$$

where c is the specific chemical reaction, r is the reactant, p_1 and p_2 are the products, and s is the collision partner. Each of the dissociation reactions with corresponding forward reactions rates are shown in Table 2.2.

Table 2.2: Dissociation Rates

	Reaction	Partner	$C_f \left(\frac{m^3}{mol \times s}\right)$	η	$\theta_d(K)$
1	$N_2 + M \Leftrightarrow 2N + M$	all molecular species	3.7×10^{15}	-1.6	113200
		all atomic species	1.11×10^{16}	-1.6	113200
2	$O_2 + M \Leftrightarrow 2O + M$	all molecular species	2.75×10^{23}	-1.0	59500
		all atomic species	8.25×10^{13}	-1.0	59500
3	$NO + M \Leftrightarrow N + O + M$	all molecular species	2.30×10^{11}	-0.5	75500
		all atomic species	4.60×10^{11}	-0.5	75500

The exchange reactions take the form of equation (2.8). The exchange reactions are shown in Table 2.3.

$$R_c = \sum_{s=1}^{ns} \left(-k_{f,c} \frac{\rho_{r1}}{M_{r1}} \frac{\rho_{r2}}{M_{r2}} + k_{b,c} \frac{\rho_{p1}}{M_{p1}} \frac{\rho_{p2}}{M_{p2}} \right) \tag{2.8}$$

Table 2.3: Exchange Rates

	Reaction	$C_f \left(\frac{m^3}{mol \times s}\right)$	η	$\theta_d(K)$
4	$N_2 + O \Leftrightarrow NO + N$	3.18×10^7	0.10	37700
5	$NO + O \Leftrightarrow N + O_2$	2.16×10^2	1.29	19220
6	$N_2 + O_2 \Leftrightarrow NO + NO$	6.69×10^{11}	-2.54	64639

Each reaction is governed by a forward and backward reaction rate determined by

equations, (2.9) and (2.10).

$$k_f = C_f T_a^{\eta} \exp(-\theta_d / T_a) \tag{2.9}$$

$$k_b = \ k_f / K_{eq} \tag{2.10}$$

Where T_a is the defining temperature for the reaction and is defined by equation (2.11).

$$T_a = \sqrt{T T_V} \tag{2.11}$$

The value of T_a shown in equation (2.11) is used for the three dissociation reactions. For the exchange reactions and backward reaction rates, $T_a \ = \ T$, is used. The equilibrium coefficient, K_{eq}, shown in equation (2.10), can be computed from a curve fit taken from Park [17] and shown in equation (2.12).

$$K_{eq} = \exp\left(\frac{A_1}{Z} + A_2 \ + A_3 ln\,(Z) \ + \ A_4 Z + A_5 Z^2\right), \ Z \ = \ \frac{10000}{T} \tag{2.12}$$

The values of the A_i coefficients can be shown in Tables 2.4 - 2.9, where N_s is the number density of species.

Table 2.4: Coefficient of A_i's for $N_2 + M \Leftrightarrow 2N + M$

N_s	A_1	A_2	A_3	A_4	A_5
10^{14}	3.490700	0.831330	4.097800	-12.728000	0.074870
10^{15}	2.072300	1.389700	2.061700	-11.828000	0.015105
10^{16}	1.606000	1.573200	1.392300	-11.533000	-0.004543
10^{17}	1.535100	1.606100	1.299300	-11.494000	-0.006980
10^{18}	1.476600	1.629100	1.215300	-11.457000	-0.009444
10^{19}	1.476600	1.629100	1.215300	-11.457000	-0.009444

Table 2.5: Coefficient of A_i's for $O_2 + M \Leftrightarrow 2O + M$

N_s	A_1	A_2	A_3	A_4	A_5
10^{14}	2.164900	0.078577	2.850800	-8.542200	0.053043
10^{15}	1.007200	0.535450	1.191100	-7.809800	0.004394
10^{16}	0.638170	0.681890	0.663360	-7.577300	-0.011025
10^{17}	0.558890	0.715580	0.553960	-7.530400	-0.014089
10^{18}	0.515000	0.732860	0.490960	-7.502500	-0.015938
10^{19}	0.507650	0.735750	0.480420	-7.497900	-0.016247

Table 2.6: Coefficient of A_i's for $NO + M \Leftrightarrow N + O + M$

N_s	A_1	A_2	A_3	A_4	A_5
10^{14}	1.810300	1.960700	3.571600	-7.362300	0.083861
10^{15}	0.913540	2.316000	2.288500	-6.796900	0.046338
10^{16}	0.641830	2.425300	1.902600	-6.627700	0.035151
10^{17}	0.553880	2.460000	1.776300	-6.572000	0.031445
10^{18}	0.524550	2.471500	1.734200	-6.553400	0.030209
10^{19}	0.509890	2.477300	1.713200	-6.544100	0.029591

Table 2.7: Coefficient of A_i's for $N_2 + O \Leftrightarrow NO + N$

N_s	A_1	A_2	A_3	A_4	A_5
10^{14}	1.326100	0.752680	1.247400	-4.185700	0.021840
10^{15}	1.065300	0.854170	0.870930	-4.018800	0.010721
10^{16}	0.967940	0.891310	0.729100	-3.955500	0.006488
10^{17}	0.976460	0.890430	0.745720	-3.964200	0.007123
10^{18}	0.961880	0.896170	0.724790	-3.955000	0.006509
10^{19}	0.969210	0.893290	0.735310	-3.959600	0.006818

Table 2.8: Coefficient of A_i's for $NO + O \Leftrightarrow N + O_2$

N_s	A_1	A_2	A_3	A_4	A_5
10^{14}	0.354380	-1.882100	-0.721110	-1.1797000	-0.030831
10^{15}	0.093613	-1.780600	-1.097500	-1.012800	-0.041949
10^{16}	-0.003732	-1.743400	-1.239400	-0.949520	-0.046182
10^{17}	0.004815	-1.744300	-1.222700	-0.958240	-0.045545
10^{18}	-0.009758	-1.738600	-1.243600	-0.949000	-0.046159
10^{19}	-0.002428	-1.741500	-1.233100	-0.953650	-0.45850

Table 2.9: Coefficient of A_i's for $N_2 + O_2 \Leftrightarrow NO + NO$

N_s	A_1	A_2	A_3	A_4	A_5
10^{14}	-2.581100	2.286300	-5.094600	-2.037800	-0.121920
10^{15}	-2.581100	2.286300	-5.094600	-2.037800	-0.121920
10^{16}	-2.581100	2.286300	-5.094600	-2.037800	-0.121920
10^{17}	-2.581100	2.286300	-5.094600	-2.037800	-0.121920
10^{18}	-2.581100	2.286300	-5.094600	-2.037800	-0.121920
10^{19}	-2.581100	2.286300	-5.094600	-2.037800	-0.121920

The chemical production source terms for each species can be found and is shown in equation (2.13).

$$W_{N_2} = M_{N_2}(R_1 + R_4 + R_6) \tag{2.13a}$$

$$W_{O_2} = M_{O_2}(R_2 + R_6) \tag{2.13b}$$

$$W_{NO} = M_{NO}(R_3 - R_4 + R_5 - 2R_6) \tag{2.13c}$$

$$W_N = M_N(-2R_1 - R_3 - R_4 - R_5) \tag{2.13d}$$

$$W_O = M_O(-2R_2 - R_3 + R_4 + R_5) \tag{2.13e}$$

The Landau-Teller formulation, equation (2.14) is used to calculate the source term in the vibration energy equation which represents the exchange of energy between the translation-rotation and vibration energies.

$$Q_{T-V,s} = \rho_s \frac{e_{v,s}(T) - e_{v,s}(T_V)}{< \tau_s > + \tau_{cs}} \tag{2.14}$$

Where $< \tau_s >$ is the Landau-Teller vibration relaxation time given by Lee [19] and defined in equation (2.15).

$$< \tau_s > = \frac{\sum_{r=1}^{ns} X_r}{\sum_{r=1}^{ns} X_r / \tau_{sr}} \tag{2.15}$$

X_r is the molar concentration of species r.

The variable, τ_{sr}, is obtained from Millikan and White [20] using equation (2.16).

$$\tau_{sr} = \frac{1}{p} \exp\left[A_{sr}\left(T^{-1/3} - 0.015\mu_{sr}^{1/4}\right) - 18.42\right], \; p \; in \; atm \tag{2.16}$$

$$A_{sr} = 1.16 \times 10^{-3} \mu_{sr}^{1/2} \theta_{v,c}^{4/3} \tag{2.17}$$

$$\mu_{sr} = \frac{M_s M_r}{M_s + M_r} \times 1000 \tag{2.18}$$

$\theta_{v,c}$ is the characteristic temperature corresponding to the energy level of the first excited vibrational mode. τ_{cs} is from Park [17] and is used to more accurately model the relaxation time in areas of high temperatures occurring just downstream of the bow shock.

$$\tau_{cs} = 1/C_s \sigma_v N_s \tag{2.19}$$

$$C_s = \sqrt{8RT/\pi M_s} \tag{2.20}$$

$$\sigma_v = 10^{-21}(50000/T)^2 \tag{2.21}$$

Detailed models of the transport coefficients are neglected here because they are not

important for HSDT. For the preliminary/conceptual design of hypersonic vehicles, one can neglect the transport terms (mass, momentum, and energy). Hence, an approximate solution of flow field can be obtained by solving the inviscid governing equations. Therefore, the governing equation of HSDT for general hypersonic flow is as follows.

$$\frac{\partial U}{\partial t} + \frac{\partial F_j}{\partial x_j} = W \tag{2.22}$$

For specific cases of hypersonic flow, modification of equation (2.22) is necessary depending on the geometric body and flow models of air (perfect gas, diatomic dissociating gas, and general equilibrium gas and even non-equilibrium flow).

CHAPTER 3

HSDT FOR PERFECT GAS FLOW

3.1 Modification of Governing Equations for Flows over a Wedge and a Cone

For HSDT, the geometric body is described by $B(x, y, z) = 0$ and the shock wave relations are described by $S(x, y, z) = 0$, this coordinate system is illustrated in Fig. 3.1. The full governing equations are the equations of motion, equation (2.22). For steady per-

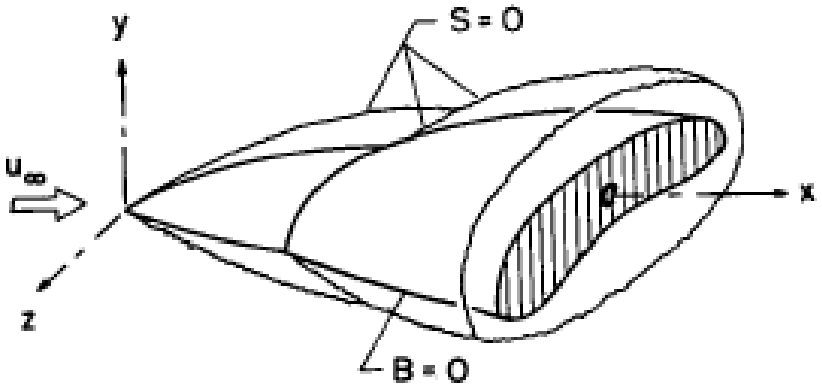

Figure 3.1: HSDT Coordinate System

fect gas flow, the temporal derivative, source term and the vibration energy equation are neglected. The total energy equation is reduced to the isentropic equation. The other assumptions as previously stated are 1.) viscosity and heat conduction are neglected, 2.) the body is assumed to be thin, and 3.) the freestream Mach number is considered hypersonic.

The full governing equations can be written in the following Cartesian coordinates.

$$(\rho u)_x + (\rho v)_y + (\rho w)_z = 0 \tag{3.1a}$$

$$uu_x + vu_y + wu_z + (\frac{P_x}{\rho}) = 0 \tag{3.1b}$$

$$uv_x + vv_y + wv_z + (\frac{P_y}{\rho}) = 0 \tag{3.1c}$$

$$uw_x + vw_y + ww_z + (\frac{P_z}{\rho}) = 0 \tag{3.1d}$$

$$u(\frac{P}{\rho^\gamma})_x + v(\frac{P}{\rho^\gamma})_y + w(\frac{P}{\rho^\gamma})_z = 0 \tag{3.1e}$$

The full equations of motion can be simplified to the first-order HSDT equation by normalizing with respect to τ. This is achieved by introducing new independent variables that are non-dimensionalized. The non-dimensional variables are shown in equation (3.2).

$$\bar{x} = x; \quad \bar{r} = \frac{r}{\tau}; \quad \bar{u} = \frac{\left[\frac{u}{U_\infty} - 1\right]}{\tau^2}; \quad \bar{v} = \frac{v}{U_\infty \tau}; \quad \bar{p} = \frac{p}{p_\infty \gamma M_\infty^2 \tau^2} \quad \bar{\rho} = \frac{\rho}{\rho_\infty} \tag{3.2}$$

By introducing these equations into equation (3.1), and removing the terms that contain τ^2, the first-order HSDT equations are obtained and are shown in equation (3.3).

$$(\bar{\rho})_{\bar{x}} + (\bar{\rho}\bar{v})_{\bar{y}} + (\bar{\rho}\bar{w})_{\bar{z}} = 0 \tag{3.3a}$$

$$\bar{u}_{\bar{x}} + \bar{v}\bar{u}_{\bar{y}} + \bar{w}\bar{u}_{\bar{z}} + (\frac{\bar{P}_{\bar{x}}}{\bar{\rho}}) = 0 \tag{3.3b}$$

$$\bar{v}_{\bar{x}} + \bar{v}\bar{v}_{\bar{y}} + \bar{w}\bar{v}_{\bar{z}} + (\frac{\bar{P}_{\bar{y}}}{\bar{\rho}}) = 0 \tag{3.3c}$$

$$\bar{w}_{\bar{x}} + \bar{v}w_{\bar{y}} + \bar{w}\bar{w}_{\bar{z}} + (\frac{\bar{P}_{\bar{z}}}{\bar{\rho}}) = 0 \tag{3.3d}$$

$$(\frac{\bar{P}}{\bar{\rho}^\gamma})_{\bar{x}} + \bar{v}(\frac{\bar{P}}{\bar{\rho}^\gamma})_{\bar{y}} + w(\frac{\bar{P}}{\bar{\rho}^\gamma})_{\bar{z}} = 0 \tag{3.3e}$$

From the first-order HSDT equations, the boundary conditions for the upstream flow and tangent to the body can be obtained and are shown in equation (3.4) and (3.5), respec-

tively.

$$\left.\begin{array}{c} \bar{u} = \ \bar{v} = \ \bar{w} \to 0 \\ \bar{P} \to \dfrac{1}{\gamma M^2 \tau^2} \\ \bar{\rho} \to 1 \end{array}\right\} \ as \ \bar{x} \ \to \ -\infty \tag{3.4}$$

$$B_{\bar{x}} + v\bar{B}_{\bar{y}} + w\bar{B}_{\bar{z}} = 0 \text{ at } \bar{B} = 0 \tag{3.5}$$

The conditions at the shock, when $\bar{S} = 0$ for tangential momentum, mass, normal momentum, energy and the second law of thermodynamics are shown in equation (3.6), respectively.

$$\frac{[\bar{u}]}{S_{\bar{x}}} = \ \frac{[\bar{v}]}{S_{\bar{y}}} = \frac{[\bar{w}]}{S_{\bar{z}}} \tag{3.6a}$$

$$\left[\bar{\rho}\left(\bar{S}_{\bar{x}} + v\bar{S}_{\bar{y}} + w\bar{S}_{\bar{z}}\right)\right] = 0 \tag{3.6b}$$

$$\left[\bar{\rho}\left(\bar{S}_{\bar{x}} + v\bar{S}_{\bar{y}} + w\bar{S}_{\bar{z}}\right)^2 + \left(\bar{S}_{\bar{y}}^2 + \bar{S}_{\bar{z}}^2\right)\bar{p}\right] = 0 \tag{3.6c}$$

$$\left[\frac{1}{2}\left(\bar{S}_{\bar{x}} + v\bar{S}_{\bar{y}} + w\bar{S}_{\bar{z}}\right)^2 + \frac{\gamma}{\gamma - 1}\left(\bar{S}_{\bar{y}}^2 + \bar{S}_{\bar{z}}^2\right)\frac{\bar{p}}{\bar{\rho}}\right] = 0 \tag{3.6d}$$

$$\left[\frac{\bar{p}}{\bar{\rho}^{\bar{\gamma}}}\right] \geq 0 \tag{3.6e}$$

The geometric bodies that are to be considered will be either planar or axially symmetric. For this reason, the coordinates x and r are introduced into the governing equations, where r is the Cartesian coordinate y for plane flow. In the case of axially symmetric flow, v represents the velocity component in the r direction or the radial velocity for axially symmetric flow. The equations are modified in accordance with this coordinate system and become equation (3.7).

$$\bar{\rho}_{\bar{x}} + (\bar{\rho}\bar{v})_{\bar{r}} + \sigma\frac{\bar{\rho}\bar{v}}{\bar{r}} = 0 \tag{3.7a}$$

$$\bar{v}_{\bar{x}} + (\bar{v}\bar{v})_{\bar{r}} + \sigma\frac{\bar{p}_{\bar{x}}}{\rho} = 0 \tag{3.7b}$$

$$\left(\frac{\bar{p}}{\bar{\rho}^{\gamma}}\right)_{\bar{x}} + \bar{v}\left(\frac{\bar{p}}{\bar{\rho}^{\gamma}}\right)_{\bar{r}} = 0 \tag{3.7c}$$

In the continuity equation, the difference between plane flow and axially symmetric flow is $\sigma = 0$ and $\sigma = 1$, respectively.

The surface of the body can now be described by $r = \tau b(x)$. For the examples considered, the shock wave will be a single bow shock wave which can be described as $r = \tau s(x)$ as illustrated in Fig. 3.2. The freestream conditions are shown in equation (3.4).

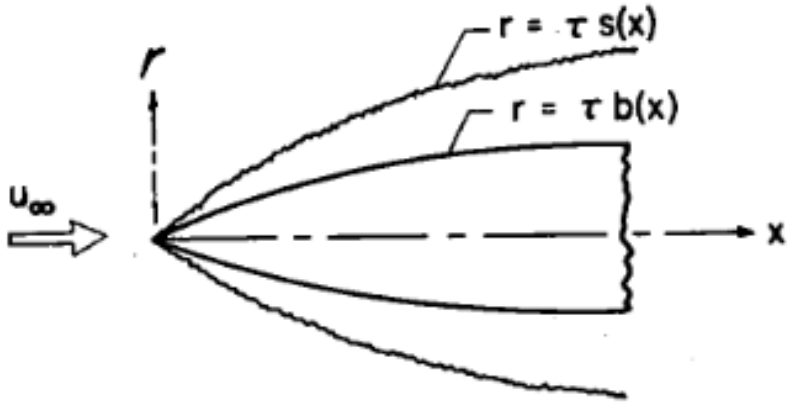

Figure 3.2: Notation for Plane or Axially Symmetric Flow [1]

The velocity condition at the surface of the body is shown in equation (3.8).

$$\bar{v} = b'(\bar{x}) \;\; at \; \bar{r} = b(\bar{x}) \tag{3.8}$$

The conditions at the shock wave are shown in equation (3.6) and are easily modified using previous research done by the Ames Staff [21]. Equations 128, 129 and 136 from [22]

are modified with HSDT and are reduced to equation (3.9),

$$\left.\begin{aligned} \bar{v} &= \frac{2}{\gamma+1}\,\frac{k^2-1}{k^2}s'(x) \\ \bar{p} &= \frac{2\gamma k^2-(\gamma-1)}{\gamma(\gamma+1)k^2}s'^2(x) \\ \bar{\rho} &= \frac{(\gamma+1)k^2}{2+(\gamma-1)k^2} \end{aligned}\right\} \; at\ \bar{r}=s(\bar{x}) \tag{3.9}$$

where $k = M\tau s'(\bar{x})$, is the hypersonic similarity parameter based on the local shock-wave slope. A stream function is now introduced to simplify the governing equations,

$$\left.\begin{aligned} \bar{r}^{\,\sigma}\bar{\rho} &= \psi_{\bar{r}} \\ \bar{r}^{\,\sigma}\bar{\rho}\bar{v} &= -\psi_{\bar{x}} \end{aligned}\right\} \tag{3.10}$$

so that

$$\left.\begin{aligned} \bar{v} &= -\frac{\psi_{\bar{x}}}{\psi_{\bar{r}}} \\ \bar{\rho} &= \frac{\psi_{\bar{r}}}{\bar{r}^{\,\sigma}} \end{aligned}\right\} \tag{3.11}$$

The energy equation, equation (3.7c) then states that $\bar{p}/\bar{\rho}^{\gamma}$ is a function of the stream function, ψ. This is true because entropy is constant along a streamline after the shock wave. Equations (3.10) and (3.11) are now substituted into the momentum equation, equation (3.7b). The momentum equation now becomes equation (3.12).

$$\psi_{\bar{r}}^2\psi_{\bar{x}\bar{x}} - 2\psi_{\bar{x}}\psi_{\bar{r}}\psi_{\bar{x}\bar{r}} + \psi_x^2\psi_{\bar{r}\bar{r}} = \begin{cases} \psi_{\bar{r}}^{\gamma+1}\left(\gamma\omega\psi_{\bar{r}\bar{r}}+\omega'\right)\psi_{\bar{r}}^2 \text{ for plane flow} \\ \dfrac{\psi_{\bar{r}}^{\gamma+1}}{\bar{r}^{\gamma-1}}\left[\gamma\omega\left(\psi_{\bar{r}\bar{r}}-\dfrac{\psi_{\bar{r}}}{\bar{r}}\right)\omega'\psi_{\bar{r}}^2\right] \text{ for axially symmetric flow} \end{cases} \tag{3.12}$$

where

$$\omega(\psi) = \frac{\bar{p}}{\bar{\rho}^{\gamma}} \tag{3.13}$$

The pressure is given by

$$\bar{p} = \omega\bar{\rho}^{\gamma} = \omega\left(\frac{\psi_{\bar{r}}}{\bar{r}^{\sigma}}\right)^{\gamma} \tag{3.14}$$

Further modifications to these equations for plane and axially symmetric flows are carried out for specific cases in the following sections of the paper.

3.2 Result of Hypersonic Flow over a Plane Wedge

For a plane wedge, the flow field around the plane wedge has conical streamlines and the stream function can be described by equation (3.15).

$$\psi\left(\bar{x},\bar{r}\ \right) = \bar{x}f\left(\theta\right) \tag{3.15}$$

The equation for plane flow, equation (3.12) is modified in accordance with the stream function and becomes equation (3.16).

$$f''\left[f^2 - \gamma\omega_0 f'^{(\gamma+1)}\right] = 0 \tag{3.16}$$

Where ω_0 is determined by equation (3.17).

$$\omega_0 = \frac{2\gamma K_0^2 - (\gamma-1)}{\gamma\left(\gamma+1\right)K_0^2}\left[\frac{2+(\gamma-1)\,K_0^2}{(\gamma+1)\,K_0^2}\right]^{\gamma} \tag{3.17}$$

$$K_0 = M\tau \tag{3.18}$$

The conditions at the shock are shown in equation (3.19).

$$f\left(1\right) = 1 \tag{3.19a}$$

$$f'(1) = \frac{(\gamma+1)\,K_0^2}{2+(\gamma-1)\,K_0^2} \tag{3.19b}$$

By applying these conditions, the ordinary differential equation (3.16) can be solved. In his comparison of the analytical solution to experimental data, van Dyke found that as flow became supersonic the approximation became less accurate [1, 5]. As a result, he applied the unified supersonic-hypersonic theory to his solution by replacing $M\delta$ with $\beta\delta$ and so that the coefficient of pressure can now be found in equation (3.20).

$$C_p = \delta^2 \left[\frac{\gamma+1}{2} + \sqrt{\left(\frac{\gamma+1}{2}\right)^2 + \frac{4}{\beta^2\delta^2}} \right] \tag{3.20}$$

β is shown in equation (3.21).

$$\beta = \sqrt{M^2 - 1} \tag{3.21}$$

For comparison, the coefficient of pressure over a plane wedge from oblique shock theory can be found in equation (3.22).

$$C_p = \frac{4}{\gamma+1}\left(sin^2\theta_w - \frac{1}{M^2} \right) \tag{3.22}$$

θ_w can be found from solving the $\theta - \beta - M$ equation, shown in equation (3.23), where β has been replaced by θ_w.

$$\tan\delta = 2\cot(\theta_w)\frac{(M^2\sin^2\theta_w) - 1}{M^2(\gamma + \cos 2\theta_w) + 2} \tag{3.23}$$

The plane wedge model was solved in MATLAB and was run for a range of Mach numbers from 5 to 15 for three half angles: 5°, 10°and 15°. The results of HSDT and oblique shock theory for perfect gas flow ($\gamma = 1.40$) are shown in Fig. 3.3.

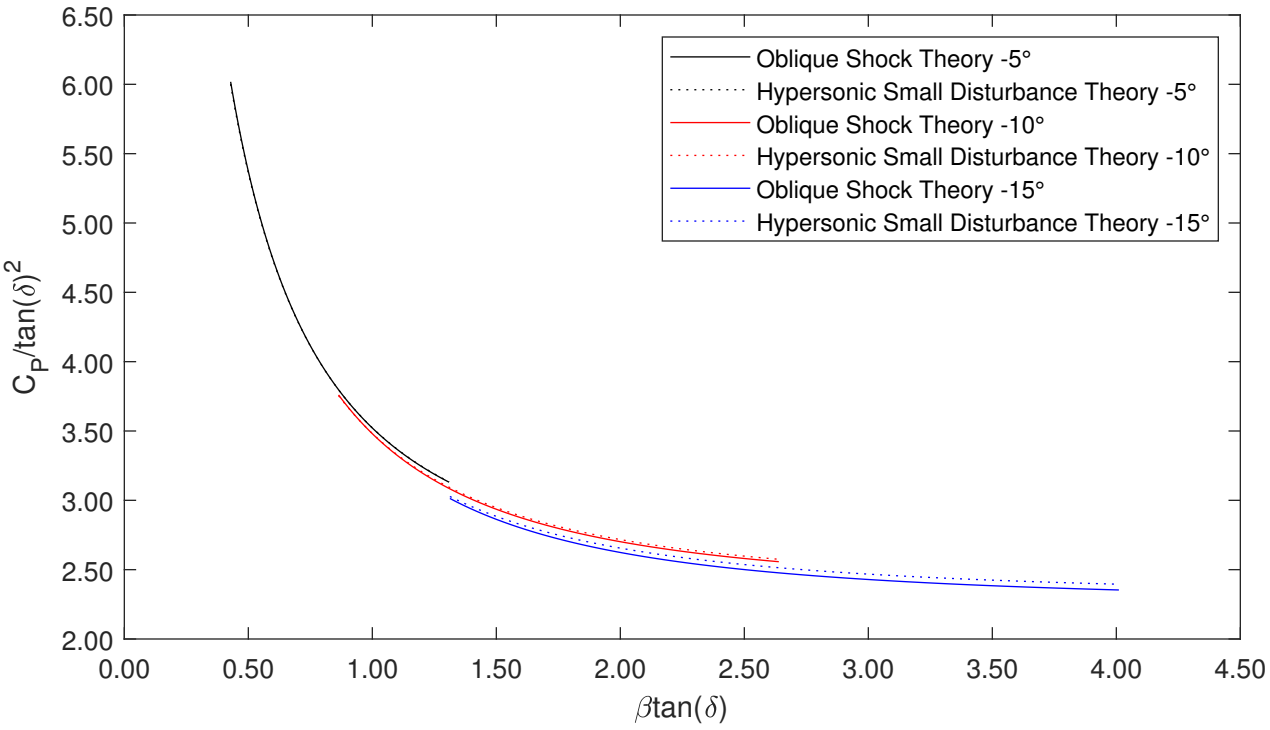

Figure 3.3: Surface Pressure on Wedge ($\delta = 5°, 10°, \text{and } 15°$)

For the plane wedge, it can be shown that the results for oblique shock theory and HSDT are in agreement. However, as the value of δ is increased a small deviation begins to take place between the two theories. This difference is quantifiable by computing the Root Mean Square (RMS), shown in equation (3.24).

$$RMS = \sqrt{\frac{1}{n}\sum_{i=1}^{n}(Cp_{1i} - Cp_{2i})^2} \tag{3.24}$$

Shown in Table 3.1 are the RMS values and percent differences for each plane wedge case, which shows that as the angle is increased, there is small deviation between the two theories.

Table 3.1: Plane Wedge RMS and Percent Difference

Wedge Angle	RMS	Percent Difference
5°	4.986×10^{-3}	0.075
10°	1.308×10^{-2}	0.438
15°	3.529×10^{-2}	1.379

3.3 Result of Hypersonic Flow over a Circular Cone

In the current section, a model of a circular cone with perfect gas flow is used. Much like the plane wedge, the flow field around the circular cone has conical streamlines and the stream function can be shown in equation (3.25).

$$\psi\left(\bar{x}, \bar{r}\ \right) = \bar{x}^2 f\left(\theta\right) \tag{3.25}$$

The equation for asymmetrical flow, equation (3.12) is modified in accordance with the stream function and becomes equation (3.26).

$$4f^2 f'' - 2f' f^2 = \ \gamma\omega_0 \frac{f'^{(\gamma+1)}}{\theta^{(\gamma-1)}} \left(f'' - \frac{f\prime}{\theta}\right) \tag{3.26}$$

The conditions at the shock are shown in equation (3.27).

$$f\left(1\right) = \ 1/2 \tag{3.27a}$$

$$f'(1) = \frac{\left(\gamma+1\right) K_0^2}{2 + \left(\gamma-1\right) K_0^2} \tag{3.27b}$$

By solving the nonlinear ordinary differential equation shown in equation (3.26) and applying the boundary conditions, the values of f and f' can be found. The pressure coeffi-

cient at the circular cone can then be found and is shown in equation (3.28).

$$C_p = \ 2\delta^2 \left[\frac{\omega_0}{b^2} \left(\frac{f'}{\theta} \right)^{\gamma} - \frac{1}{\gamma \beta^2 \delta^2} \right] \tag{3.28}$$

For comparison, the coefficient of pressure over a circular cone from oblique shock theory is shown in equation (3.29).

$$C_p = \frac{2}{\gamma M^2} \left(\frac{P_c}{P_1} - 1 \right) \tag{3.29}$$

Where $\frac{P_c}{P_1}$ and $\frac{P_2}{P_1}$ is found in equations (3.30) and (3.31), respectively.

$$\frac{P_c}{P_1} = \frac{\left(1 + \frac{\gamma - 1}{2M_C}\right)^{\frac{-\gamma}{\gamma - 1}}}{\left(1 + \frac{\gamma - 1}{2M_2}\right)^{\frac{-\gamma}{\gamma - 1}}} \frac{P_2}{P_1} \tag{3.30}$$

M_C is the Mach at the surface of the cone and can be found by solving the Taylor Maccoll Equations.

$$\frac{P_2}{P_1} = 1 + \frac{2\gamma}{\gamma + 1} \left(M^2 sin^2 \beta - 1 \right) \tag{3.31}$$

Similar to the plane wedge case, the circular cone model was solved in MATLAB and run for a range of Mach numbers from 5 to 15 for three half angles: 5°, 10°and 15°. The results of HSDT and oblique shock theory for perfect gas flow are shown in Fig. 3.4.

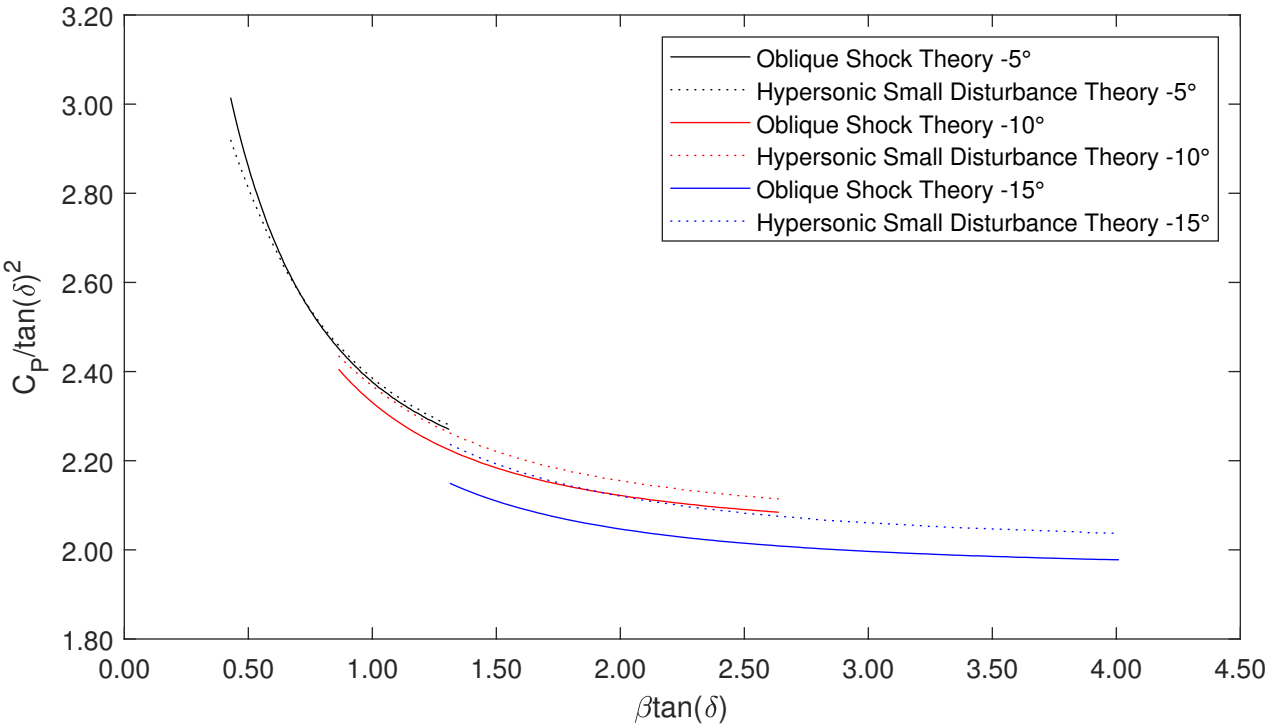

Figure 3.4: Surface Pressure on Circular Cone ($\delta = 5°, 10°,$ and $15°$)

Much like the plane wedge, the results for a circular cone show a deviation between the oblique shock theory and HSDT. Again, this difference is quantifiable by computing the RMS, shown in equation (3.24). Shown in Table 3.2 are the RMS values and percent differences for each circular cone case, which again shows, that as the angle is increased, there is small deviation between the two theories.

Table 3.2: Circular Cone RMS and Percent Difference

Circular Cone	RMS	Percent Difference
5°	2.442×10^{-2}	0.578
10°	3.461×10^{-2}	1.571
15°	6.927×10^{-2}	3.337

3.4 Modification of Governing Equations for Hypersonic Flow over a Power-Law Shock Bodies

For a power-law shock body, the solution can be obtained by assuming the shock wave, and then iterating down towards the body surface. The applicable solution to the HSDT is obtained when flow similarity can be exhibited and the required conditions are met. The full equations of motion, equation (2.22), are subjected to a transformation of variables and are defined in their reduced form in equation (3.32).

$$\text{Continuity} \quad \frac{\partial \bar{\rho}}{\partial \bar{x}} + \frac{\partial \bar{\rho}\bar{v}}{\partial \bar{r}} + k\frac{\bar{\rho}\bar{v}}{\bar{r}} = 0 \tag{3.32a}$$

$$\text{R- Momentum} \quad \bar{\rho}\left(\frac{\partial \bar{v}}{\partial \bar{x}} + \bar{v}\frac{\partial \bar{v}}{\partial \bar{r}}\right) + \frac{\partial \bar{p}}{\partial \bar{r}} = 0 \tag{3.32b}$$

$$\text{Energy} \quad \left(\frac{\partial}{\partial \bar{x}} + \bar{v}\frac{\partial}{\partial \bar{r}}\right)\left(\frac{\bar{p}}{\bar{\rho}^{\gamma}}\right) = 0 \tag{3.32c}$$

The equations of motion, equation (3.32), can be solved when flow similarity is met and can be expressed as equation (3.33),

$$\bar{v}\left(\bar{x}, \bar{r}\ \right) = \bar{v}_s\left(\bar{x}\right)\phi\left(z\right) \tag{3.33a}$$

$$\bar{p}\left(\bar{x}, \bar{r}\ \right) = \bar{p}_s\left(\bar{x}\right) f\left(z\right) \tag{3.33b}$$

$$\bar{\rho}\left(\bar{x}, \bar{r}\ \right) = \bar{\rho}_s\left(\bar{x}\right)\psi\left(z\right) \tag{3.33c}$$

where $z = r/R$. By introducing equation (3.33), the operator, $\frac{\partial}{\partial x} + v\frac{\partial x}{\partial r}$ found in equation (3.32), becomes $\frac{\partial}{\partial x} + \frac{\bar{R}'}{\bar{R}}\left(\frac{\bar{v}_s}{\bar{R}'}\phi - z\right)\frac{\partial}{\partial z}$. For a similar solution to exist, $\frac{\bar{v}_s}{\bar{R}'}$ must be independent of $\bar{x}$. This occurs when $M_\infty \rightarrow \infty$ occurs. The flow variables can now be

described by equation (3.34).

$$\bar{v}\left(\bar{x},\bar{v}\ \right)=\frac{2}{\gamma+1}\bar{R}'\left(\bar{x}\right)\phi\left(z\right)\equiv\bar{R}'\left(\bar{x}\right)\phi\left(z\right) \tag{3.34a}$$

$$\bar{p}\left(\bar{x},\bar{r}\ \right)=\frac{2}{\gamma+1}\bar{R}'^{2}\left(x\right)f\left(z\right)\equiv\bar{R}'^{2}\left(x\right)F\left(z\right) \tag{3.34b}$$

$$\bar{\rho}\left(\bar{x},\bar{v}\ \right)=\psi\left(z\right) \tag{3.34c}$$

The governing equations, equation (3.32), are subject to the operator, equation (3.35), and can then be transformed to equation (3.36). Detailed derivations of equation (3.32) to equation (3.36) can be found in Appendix A.

$$\frac{\partial}{\partial\bar{x}}\ +\bar{v}\ \frac{\partial}{\partial\bar{r}}\ =\ \frac{\partial}{\partial\bar{x}}\ +\ \frac{\bar{R}'}{\bar{R}}\left(\Phi-z\right)\frac{\partial}{\partial z} \tag{3.35}$$

$$\frac{\bar{R}'}{\bar{R}}\left[\left(\phi-z\right)\psi'+\psi\phi'+k\frac{\psi\phi}{z}\right]=0 \tag{3.36a}$$

$$\left(\phi-z\right)\psi'+\frac{F'}{\psi}+\frac{\bar{R}\bar{R}''}{\bar{R}'^{2}}\phi=0 \tag{3.36b}$$

$$\left(\phi-z\right)\psi'\left[\frac{F'}{F}-\gamma\left(\frac{\psi'}{\psi}\right)\right]+\frac{\bar{R}\bar{R}''}{\bar{R}'^{2}}=0 \tag{3.36c}$$

Furthermore, flow similarity is satisfied when equation (3.37) is true and the boundary condition on the body can be described by equation (3.38).

$$\bar{R}=\frac{A}{m}x^{m} \tag{3.37}$$

$$r_{b}\sim x^{m} \tag{3.38}$$

When the conditions shown in equation (3.37) and (3.38) are satisfied and $M_{\infty}\ \rightarrow\ \infty$, the continuity, momentum and energy equations can be coupled together and the ordinary

differential equation, equation (3.39) can be solved to obtain the solution of the flow field.

$$(\phi - z)\,\psi' + \psi\phi' + k\frac{\psi\phi}{z} = 0 \tag{3.39a}$$

$$(\phi - z)\,\psi' + \frac{F'}{\psi} - \left(\frac{1}{m} - 1\right)\phi = 0 \tag{3.39b}$$

$$(\phi - z)\,\psi' \left[\frac{F'}{F} - \gamma\left(\frac{\psi'}{\psi}\right)\right] - 2\left(\frac{1}{m} - 1\right) = 0 \tag{3.39c}$$

The boundary conditions at the shock are shown in equations (3.40).

$$\phi\,(1) = F\,(1) = \frac{2}{\gamma + 1} \tag{3.40a}$$

$$\psi(1) = \frac{\gamma + 1}{\gamma - 1} \tag{3.40b}$$

Once equation (3.39) has been solved, the pressure coefficient at the surface of the body can then be found from equation (3.41).

$$C_p = \frac{2F\,(z_b)}{{z_b}^2} m^2 \delta^2 \left(\frac{x}{L}\right)^{2(m-1)} \tag{3.41}$$

3.5 Result of Hypersonic Flow over Power-Law Shock Bodies

The power-law shock body model is run for bodies with the body coefficients of $m = 1, 3/4, 2/3,$ and $4/7$ for four specific heat ratios of $\gamma = 1.67, 1.40, 1.15$ and 1.00. Shown in Fig. 3.5 is the slender body shape and shock shape for the body coefficients used in the model. The results of HSDT are shown in Figs. 3.6 - 3.9. It should be noted that values found in the nose region of a power-law shock body do not provide an accurate approximation. This is due to the criteria of $\tau << 1$ being violated in the nose region due to the rapid change of the slender body shape in the nose region. This was noted in the works of Townsend [23] and Lukasiewicz [24].

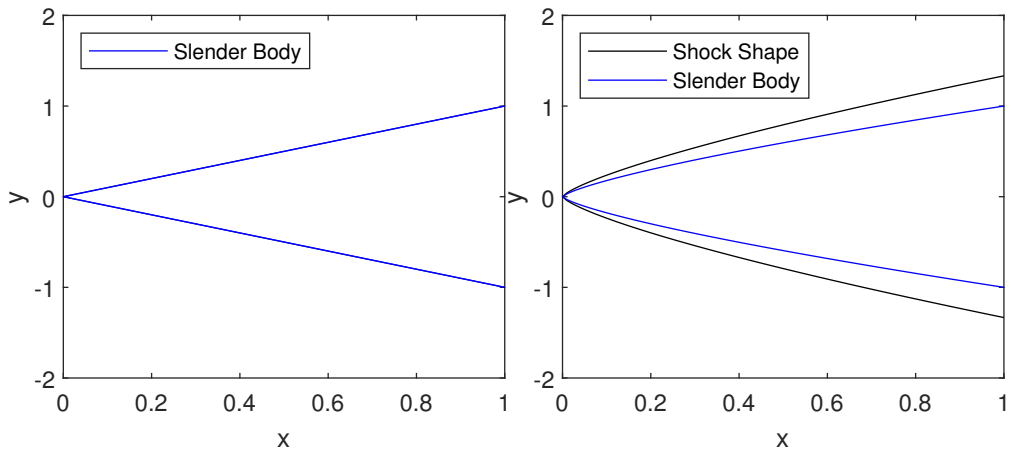

(a) $m = 1$ (b) $m = 3/4$

(c) $m = 2/3$ (d) $m = 4/7$

Figure 3.5: Body Coefficients and Shock Shape

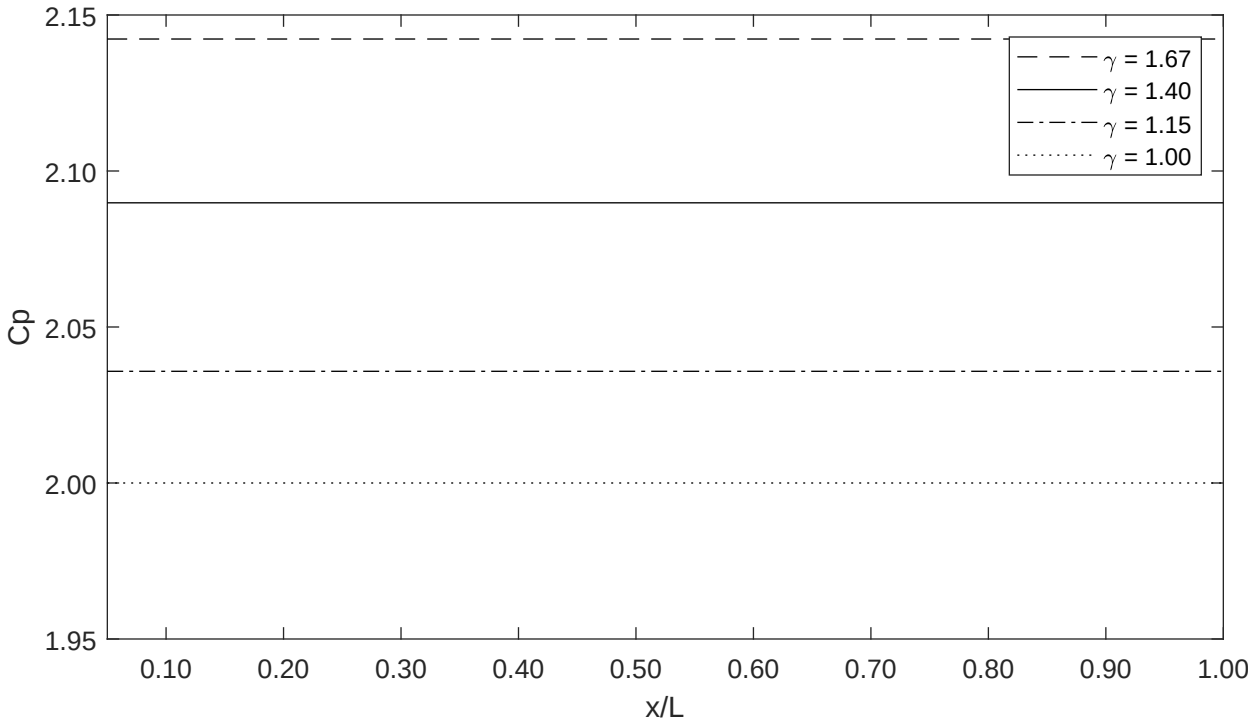

Figure 3.6: Surface Pressure on Power-Law Shock Body (m=1)

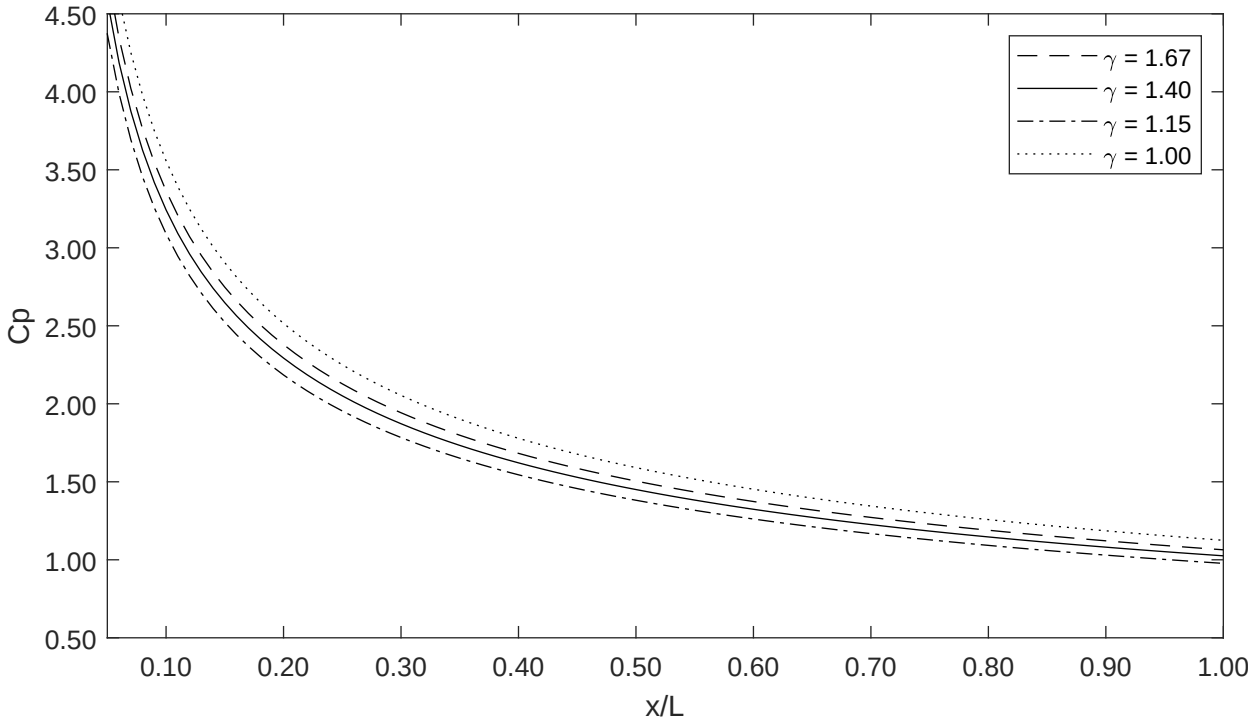

Figure 3.7: Surface Pressure on Power-Law Shock Body (m=3/4)

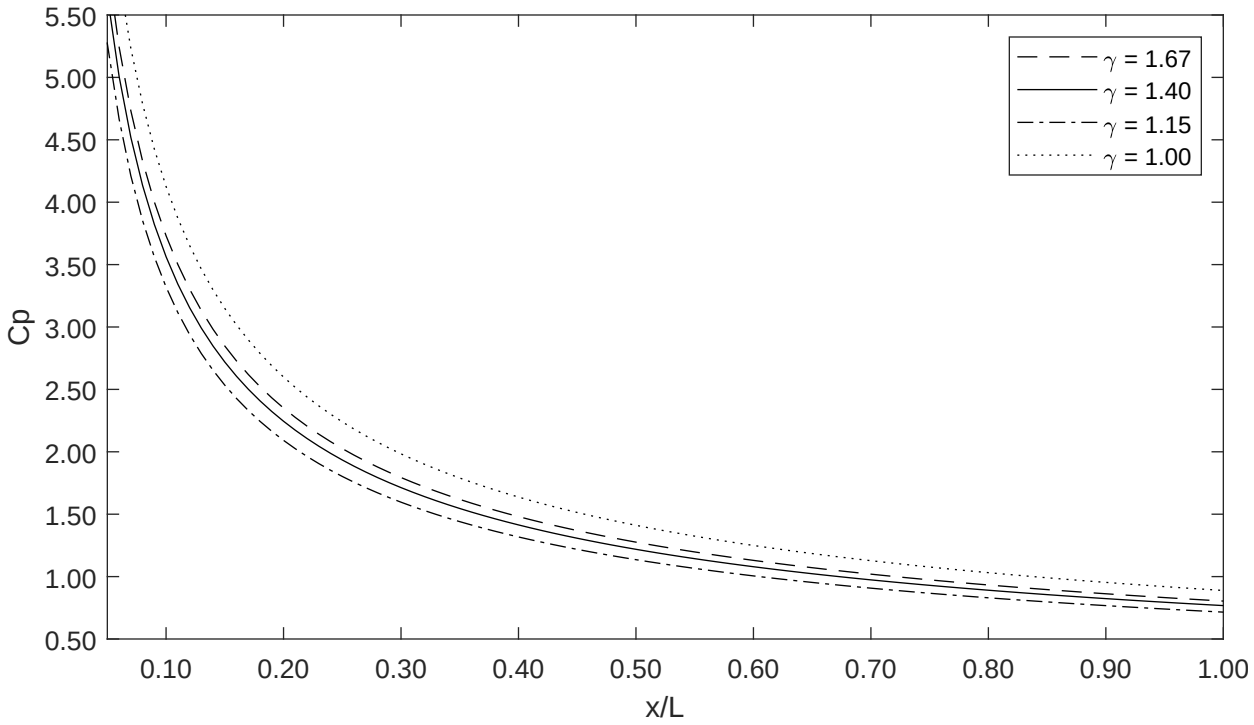

Figure 3.8: Surface Pressure on Power-Law Shock Body (m=2/3)

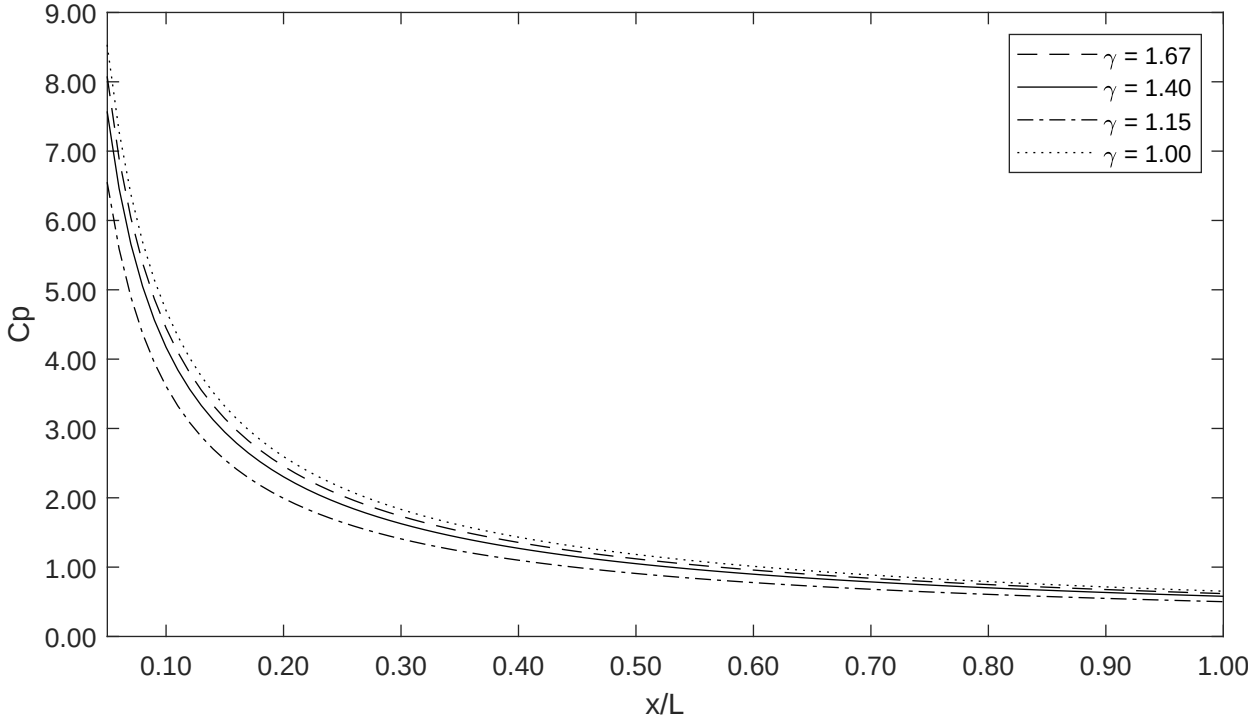

Figure 3.9: Surface Pressure on Power-Law Shock Body (m=4/7)

In Figs. 3.6 - 3.9, it can be seen that each value of γ follows the same trend. Also, as

the value of m is decreased, the coefficient of pressure at the surface of the body increases, with the highest concentration of pressure occurring just behind the nose region. This can be correlated to the drag coefficient which shows that as the body coefficient is increased, the power-law shock body will experience an increase in drag.

Shown in Figs. 3.10 - 3.11, are comparisons of the results generated for a power-law shock body of $m = 2/3$ and $4/7$ to Kubotas [12] results for the same bodies.

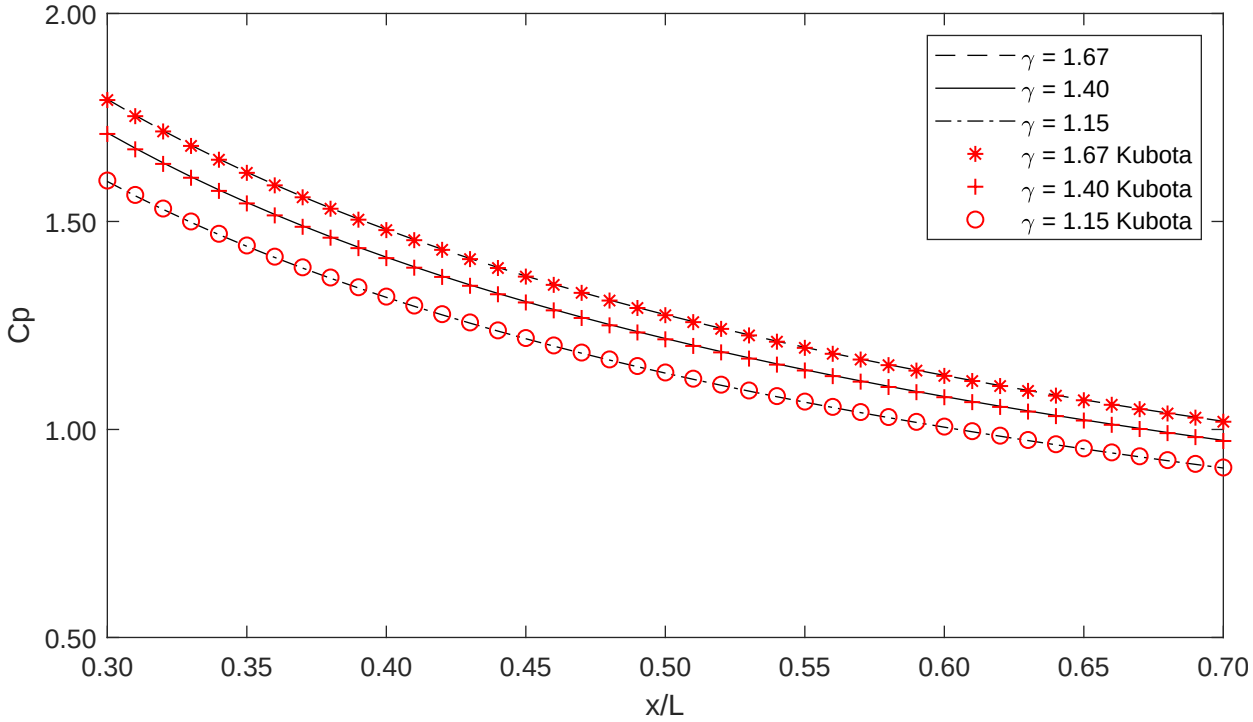

Figure 3.10: Surface Pressure on Power-Law Shock Body (m=2/3) compared to Kubota [12]

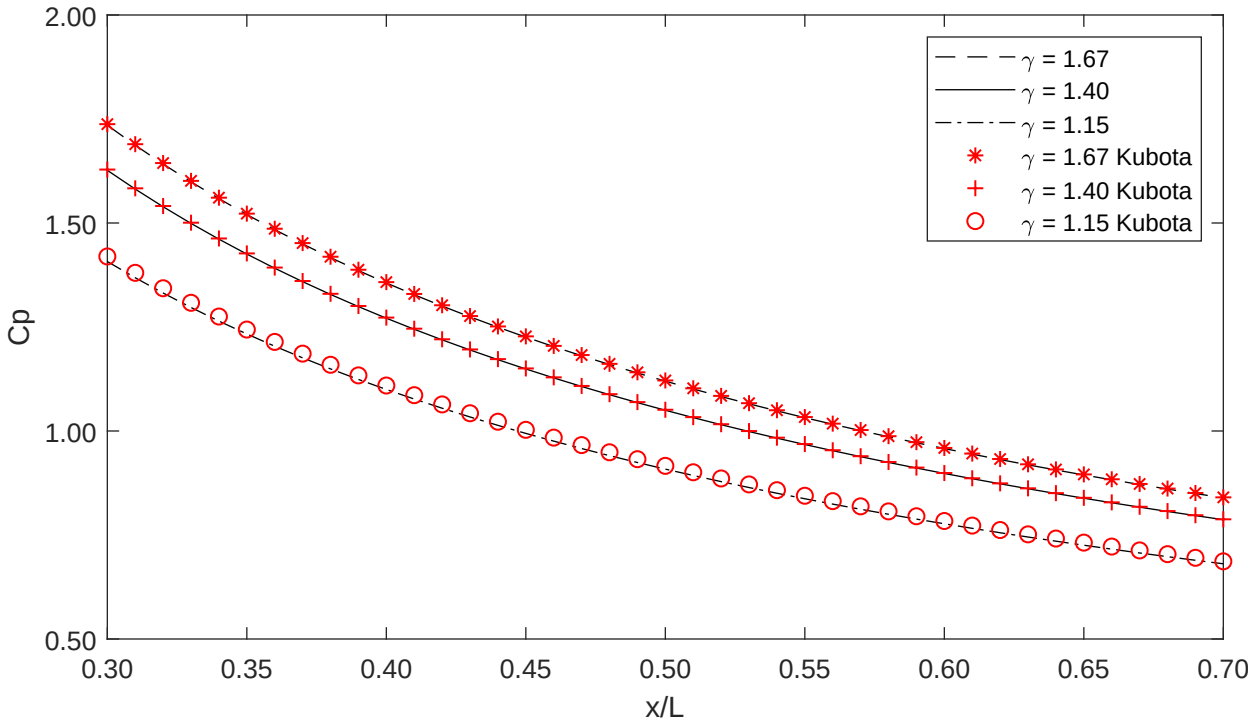

Figure 3.11: Surface Pressure on Power-Law Shock Body (m=4/7) compared to Kubota [12]

In the comparison between the MATLAB code, Appendix D, and results generated by Kubota [12], it can be seen that there is a strong agreement between the two data sets. This is able to be quantified by computing the percent difference and the RMS, shown in equation (3.24), with the results shown in Table 3.3. Additionally, the RMS and percent difference prove the accuracy of code and it's ability to quickly solve the hypersonic flow field versus a traditional approach of integrating by hand.

Table 3.3: Power-Law Shock Body Perfect Gas RMS

(a) m = 2/3

γ	RMS	Percent Difference
1.67	3.126×10^{-3}	0.105
1.40	4.319×10^{-3}	0.152
1.15	3.622×10^{-3}	0.137

(b) m = 4/7

γ	RMS	Percent Difference
1.67	6.546×10^{-3}	0.145
1.40	4.851×10^{-3}	0.115
1.15	3.153×10^{-2}	0.860

CHAPTER 4

HSDT FOR DISSOCIATING DIATOMIC GAS FLOW

4.1 Modification of Governing Equations for Hypersonic Dissociating Diatomic Gas Flow over Power-Law Shock Bodies

Much like the perfect gas solution, the solution for a dissociating diatomic gas found by Meyer [14], was obtained by assuming the shock wave and iterating down towards the body solution. For equilibrium diatomic dissociating gas, the temporal derivative, source terms, and the vibration energy equation are also neglected. The flow is isentropic with these assumptions. The full equations of motion, equation (2.22), are subjected to a transformation of variables and are defined in their reduced form in equation (4.1).

$$\text{Continuity} \quad \frac{\partial \bar{\omega}}{\partial x} + \frac{\partial \bar{\omega}\bar{v}}{\partial y} + j\frac{\bar{\omega}\bar{v}}{y} = 0 \tag{4.1a}$$

$$\text{Momentum} \quad \left(\frac{\partial}{\partial x} + \bar{v}\frac{\partial}{\partial y}\right)\bar{v} + \frac{1}{\bar{\omega}}\frac{\partial \bar{p}}{\partial y} = 0 \tag{4.1b}$$

$$\text{Energy} \quad \left(\frac{\partial}{\partial x} + \bar{v}\frac{\partial}{\partial y}\right)\bar{s} = 0 \tag{4.1c}$$

By introducing new variables, $\xi = x$ and $\eta = my/x^m$, two new operators can be defined and are shown in equation (4.2).

$$\frac{\partial}{\partial x} = \frac{\partial}{\partial \xi} - \frac{m\eta}{\zeta}\frac{\partial}{\partial \eta} \; ; \; \frac{\partial}{\partial y} = \frac{m}{\zeta^m}\frac{\partial}{\partial \eta} \tag{4.2}$$

Furthermore, a new set of functions f_1 to f_5, equation (4.3), are introduced which are in-

dependent of ξ .

$$\bar{v} = \xi^{m-1} f_1(\eta) \tag{4.3a}$$

$$\bar{p} = \xi^{2(m-1)} f_2(\eta) \tag{4.3b}$$

$$\bar{z} = \bar{p} f_3(\eta) \tag{4.3c}$$

$$\bar{h} = \bar{p} f_4(\eta) \tag{4.3d}$$

$$\frac{1}{\bar{\omega}} = f_5(\eta) \tag{4.3e}$$

These functions are then substituted into equation (4.1), which is modified with the operator, equation (4.2) to provide the third order system of differential equations, shown in equation (4.4). Detailed derivations of the equations of motion can be found in Appendix B.

$$f_1' f_5 + (\eta - 1) f_5' + \left(\frac{j}{\eta}\right) f_1 f_5 = 0 \tag{4.4a}$$

$$(m-1) f_1 - m (\eta - f_1) f_1' + m f_2' f_5 = 0 \tag{4.4b}$$

$$2 (m-1) f_2 f_3 - m (\eta - f_1) (f_2 f_3)' = 0 \tag{4.4c}$$

$$f_4 - \omega_\infty \phi \left(\omega_\infty^{-1} f_3\right) = 0 \tag{4.4d}$$

$$f_5 - \omega_\infty \chi \left(\omega_\infty^{-1} f_3\right) = 0 \tag{4.4e}$$

Where $\omega_\infty = \rho_\infty / \rho_c$ is the normalized freestream density. The boundary conditions at the shock are described by equation (4.5).

$$f_1(1) + f_5(1) - 1 = 0 \tag{4.5a}$$

$$f_2(1) - f_1(1) = 0 \tag{4.5b}$$

$$\frac{1}{2} f_1(1) + f_4(1) - 1 = 0 \tag{4.5c}$$

4.2 Approximation to a Dissociating Diatomic Gas

Equation (4.4) shows that a self-similar solution for a diatomic dissociating gas can be achieved when the equation of state takes the form of equation (4.6).

$$\frac{h}{p} = \phi \left(\frac{\psi(s)}{p} \right) \tag{4.6}$$

Where h is the non-dimensional enthalphy, p is the pressure, and s is the entropy. These variables have been normalized with respect to the characteristic energy, E_c, and density, ρ_c, this relationship is shown in equation (4.7).

$$h = \frac{H}{E_c}, p = \frac{P}{E_c \rho_c}, s = S \frac{T_c}{E_c} \tag{4.7}$$

In previous research, Lighthill [15] showed that a diatomic homonuclear gas could be approximately described by an equation of state that was defined with three adjustable constants. These constants are the characteristic density, ρ_c, characteristic energy for dissociation, E_c, and the characteristic temperature, T_c, shown in equation (4.8)

$$E_c = \frac{D}{2m_a}, \; T_c = \frac{D}{k} \tag{4.8}$$

where D, is the dissociation energy per molecule, m_a is the mass of atom and, k is Boltzmanns constant. Lighthill's equations in term of the normalized variables are shown in equation (4.9).

$$\frac{\alpha^2}{1-\alpha} = \frac{1}{\omega} \exp\left(\frac{-1}{\theta} \right) \tag{4.9a}$$

$$p = \omega\theta(1+\alpha) \tag{4.9b}$$

$$h = (4+\alpha)\,\theta + \alpha \tag{4.9c}$$

$$s = 3\ln\theta + \alpha\,(1 - 2\ln\alpha) - (1-\alpha)\ln(1-\alpha) - (1+\alpha)\ln\omega \tag{4.9d}$$

Where, α is the degree of dissociation, which can be described as the ratio of atom mass density to total mass density.

Lighthill's normalized equations, equation (4.9) does not take the form of equation (4.6) and therefore a thermodynamically consistent approximation that is in agreement with Lighthill's approximation must be used. This approximation is found by evaluating the tangent locus on a Mollier Chart and finding the points where the ratio of enthalpy and pressure is independent of the degree of dissociation. From the tangent locus, the relations shown in equations (4.10) - (4.12) are found and used to evaluate the boundary conditions for a diatomic dissociating gas.

$$\frac{h}{p} = \frac{1}{\omega}\left(3 + \alpha + \frac{1}{1-\alpha}\right) \tag{4.10}$$

$$\frac{1}{\omega} = \frac{\alpha^2}{1-\alpha}\ \exp\left(\frac{5 - 2\alpha - \alpha^2}{1-\alpha}\right) \tag{4.11}$$

$$\theta = \frac{1-\alpha}{5 - 2\alpha - \alpha^2} \tag{4.12}$$

This approximation of a dissociating diatomic gas was compared by Meyer [14] to that of Lighthills ideal dissociating gas and was found to provide a good approximation. In one instance, the pressure and density did not exceed 4% for degrees of dissociation in the range $0.2 < \alpha < 0.7$.

4.3 Solution of Dissociating Diatomic Gas

The third order nonlinear ordinary differential equations which was shown in equation (4.4) can be rewritten as

$$\sum_j a_{ij}(\eta) f_j^{'}(\eta) = b_i \quad \text{i,j} = 1, 2, 3 \tag{4.13}$$

where a_{ij},and b_i are shown in equation (4.14).

$$\begin{array}{ccc} a_{11} = f_5 & a_{12} = 0 & a_{13} = (\eta - f_1)(f_5/f_3)\frac{d\ln\chi}{d\ln(z/p)} \\ a_{21} = -m(\eta - f_1) & a_{22} = mf_5 & a_{23} = 0 \\ a_{31} = 0 & a_{32} = a_{21}f_3 & a_{33} = a_{21}f_2 \\ b_1 = -(j/\eta)f_1f_5 & b_2 = -(m-1)f_1 & b_3 = -2(m-1)f_2f_3 \end{array} \tag{4.14}$$

The value of $\mathrm{d}\ln\chi/\mathrm{d}\ln(z/p)$ was found by obtaining the corresponding value of χ, shown in equation (4.15). Similarly, the value of ϕ, shown in equation (4.16), could also be used to find $\mathrm{d}\ln\chi/\mathrm{d}\ln(z/p)$.

$$\chi = \frac{f_5}{\omega_\infty} \tag{4.15}$$

$$\phi = \frac{f_4}{\omega_\infty} \tag{4.16}$$

The value of χ was then used to interpolate a value of $\ln(z/p)$ from Table. 4.1.

Table 4.1: Arbitrary functions $\phi(z/p)$ and $\chi(z/p)$ for Dissociating Diatomic Gas [14]

$ln(z/p)$	$ln(\phi)$	$ln(\chi)$
1.5190	2.601	0.82241
2.9242	3.3360	1.8712
4.0398	4.1792	2.7043
5.0122	4.9542	3.4318
5.9106	5.6595	4.1059
6.7791	6.3449	4.7581
7.6338	7.0343	5.4116
8.5250	7.7489	6.0872
9.4618	8.5116	6.8096
10.482	9.3503	7.5973
11.627	10.303	8.4946
12.962	11.425	9.5525
14.584	12.808	10.857
16.667	14.609	12.561
19.544	17.138	14.963
23.975	21.108	18.755
32.163	28.624	25.992

By solving the nonlinear ordinary differential equations shown in equation (4.14) and applying the boundary conditions, a value of f_2 can be found at the surface of the body. The pressure coefficient at the surface of the body can then be found and is shown in equation (4.17).

$$C_p = \frac{P - P_\infty}{\frac{1}{2}\rho_\infty U_\infty^2} = \ 2\sigma^2 \xi^{2(m-1)} f_2\left(\eta_b\right) \tag{4.17}$$

4.4 Results of Dissociating Diatomic Gas HSDT

The power-law shock body model for a diatomic dissociating gas is run for a body with the power coefficients of m = 1, 3/4, 2/3, and 4/7, shown in Fig. 3.5, for three density values of $\omega_\infty = 10^{-1}, 10^{-3}$ and 10^{-5}. The results of each coefficient are shown in Figs. 4.1 - 4.4. Again, it should be noted that values found in the nose region of the body do not provide an accurate approximation due to $\tau << 1$.

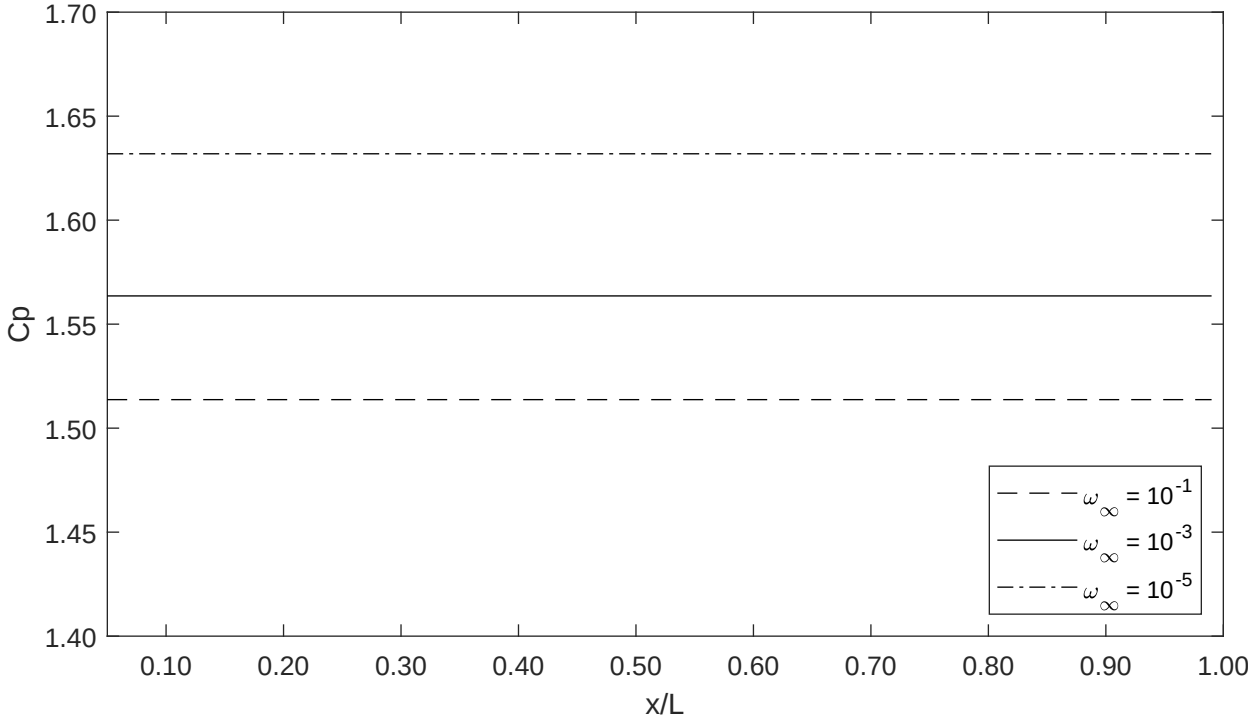

Figure 4.1: Surface Pressure on Power-Law Shock Body (m=1)

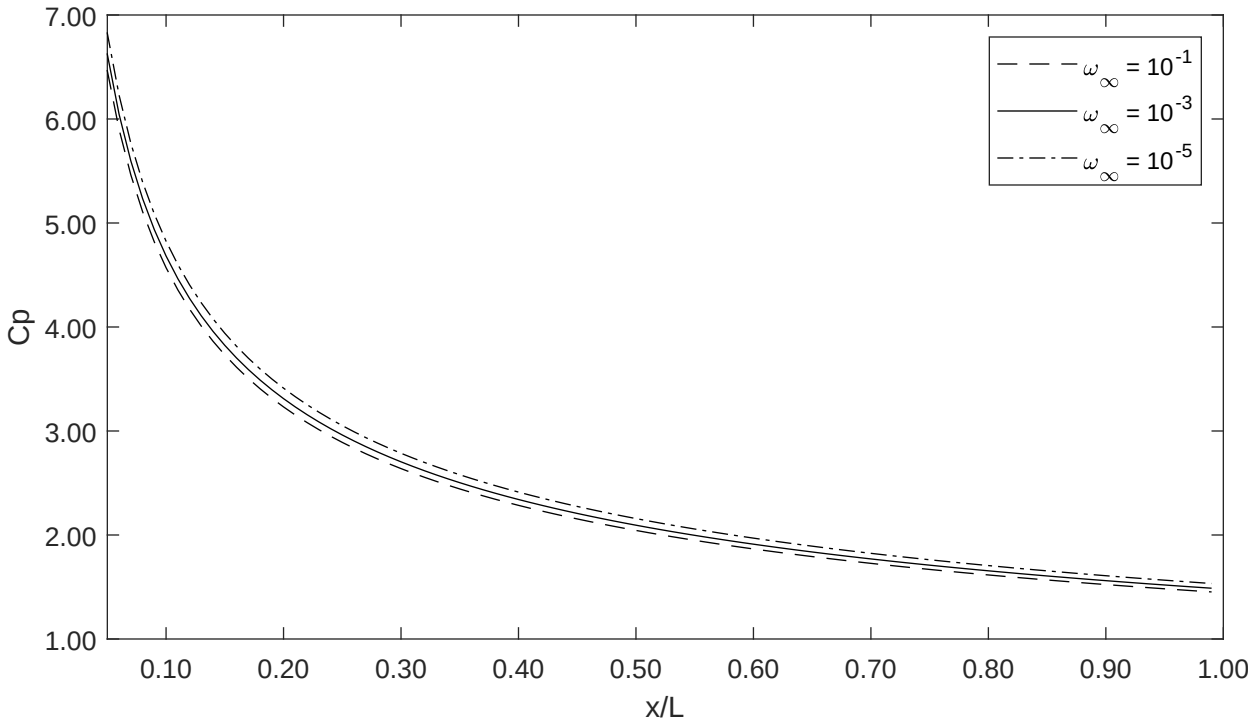

Figure 4.2: Surface Pressure on Power-Law Shock Body (m=3/4)

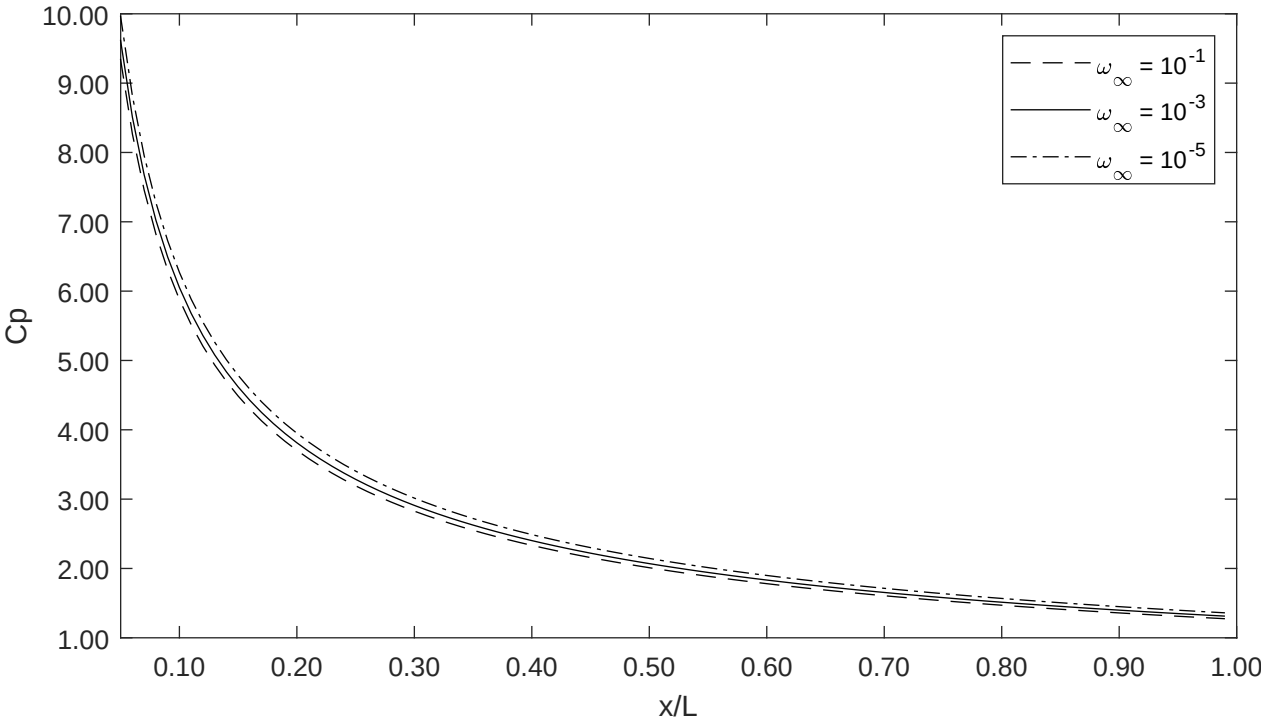

Figure 4.3: Surface Pressure on Power-Law Shock Body (m=2/3)

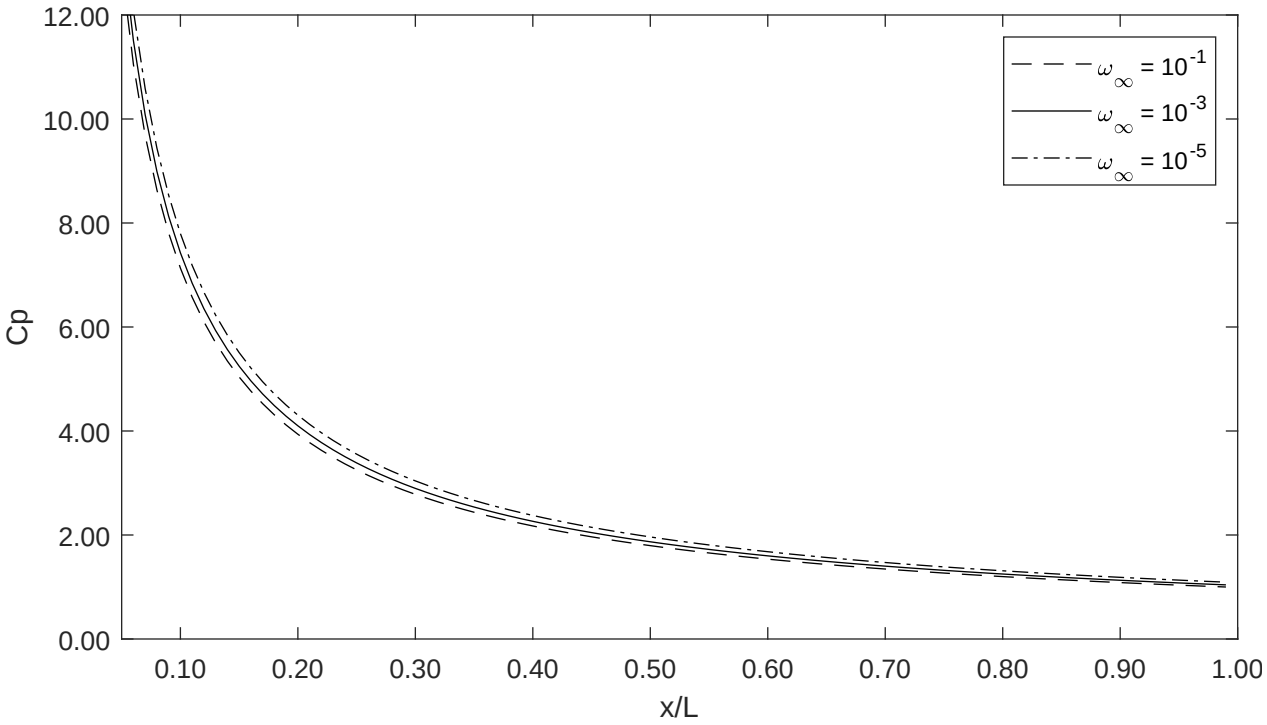

Figure 4.4: Surface Pressure on Power-Law Shock Body (m=4/7)

In Figs. 4.1 - 4.4, it can be seen that each value of ω_∞ follows the same trend as shown with the perfect gas. Also, like the perfect gas as the value of m is decreased, the coefficient of pressure at the surface of the body increases, with the highest concentration of pressure occurring just behind the nose region. Again, this can be correlated to the drag coefficient which shows that as the body coefficient is increased, the power-law shock body will experience an increase in drag.

Shown in Figs. 4.5 and 4.6 are comparisons of the generated results for a power-law shock body of $m = 2/3$ and $4/7$ to Meyers [14] results for the same bodies.

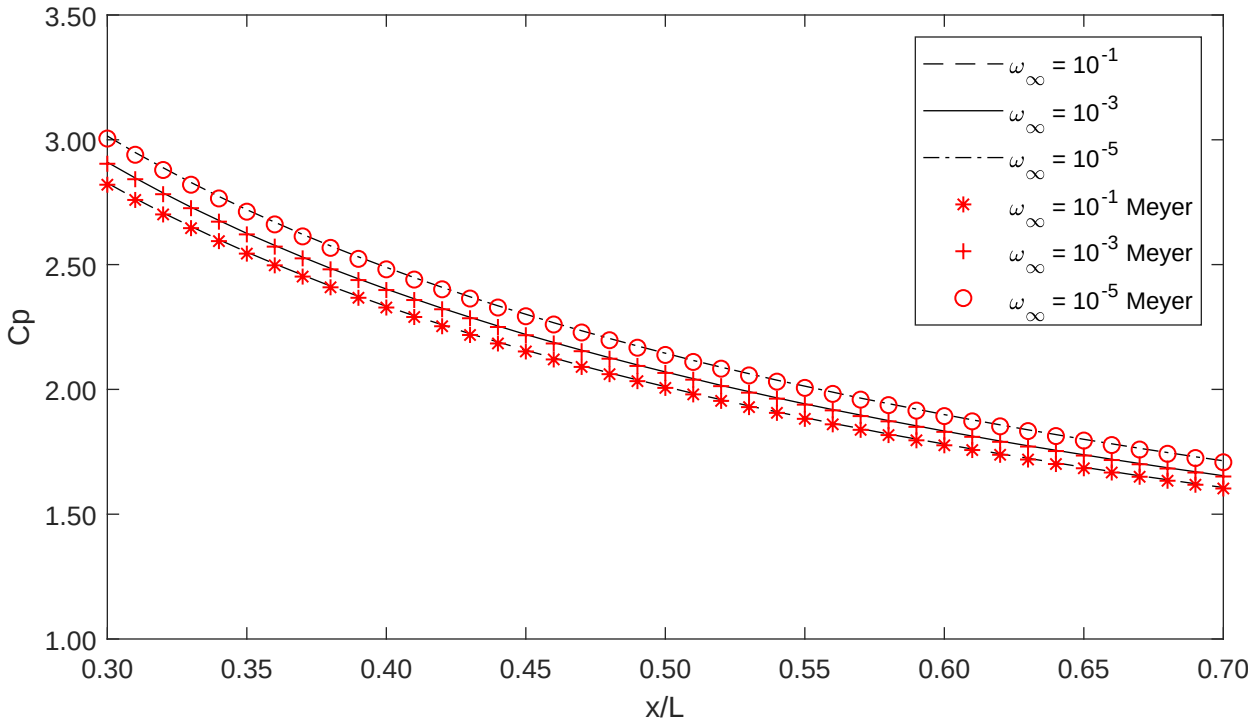

Figure 4.5: Surface Pressure on Power-Law Shock Body (m=2/3) compared to Meyer [14]

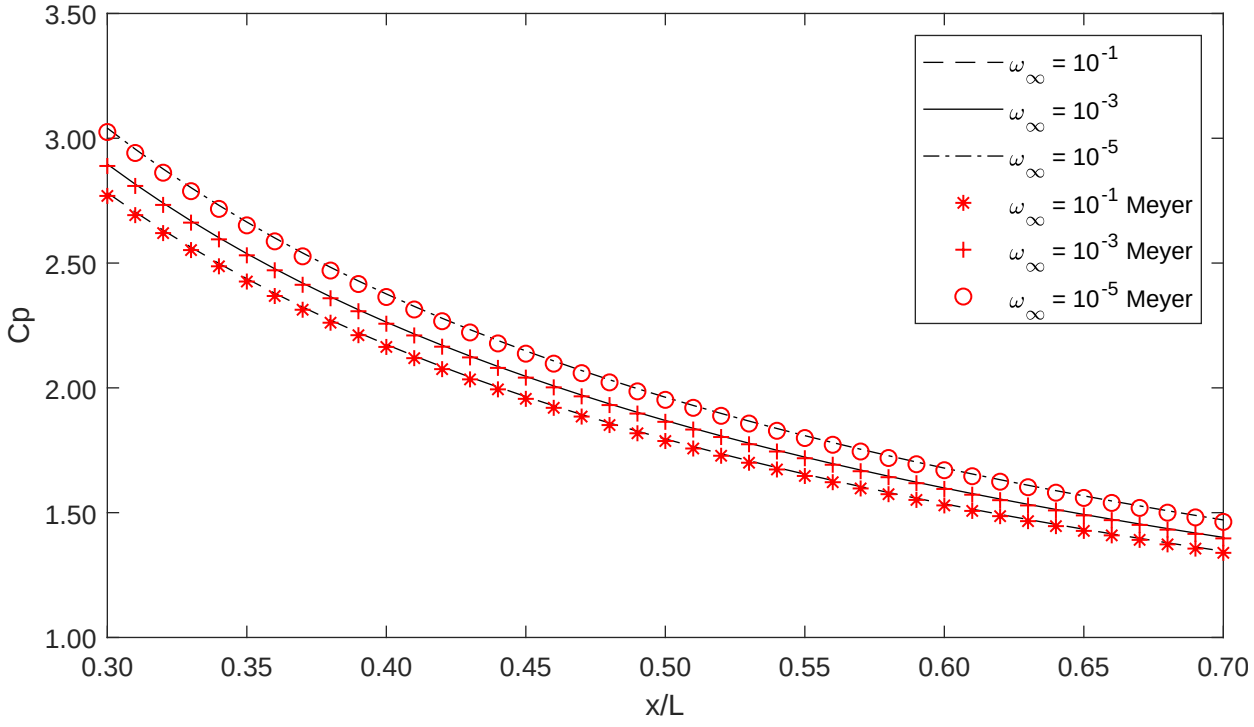

Figure 4.6: Surface Pressure on Power-Law Shock Body (m=4/7) compared to Meyer [14]

In the comparison between the MATLAB code, Appendix D, and results generated

by Meyer [14], it can be seen that there is a strong agreement between the two data sets. This is again able to be quantified by computing the percent difference and the RMS, shown in equation (3.24), with the results shown in Table 4.2. Again, the RMS and percent difference prove the accuracy of code and it's ability to quickly solve the hypersonic flow field versus a traditional approach of integrating by hand.

Table 4.2: Power-Law Shock Body Dissociating Gas RMS

(a) m = 2/3

ω_∞	RMS	Percent Difference
10^{-1}	1.146×10^{-2}	0.246
10^{-3}	8.631×10^{-3}	0.178
10^{-5}	1.560×10^{-2}	0.311

(b) m = 4/7

ω_∞	RMS	Percent Difference
10^{-1}	4.086×10^{-2}	0.453
10^{-3}	1.995×10^{-2}	0.265
10^{-5}	3.274×10^{-2}	0.517

4.5 Comparison of Perfect Gas to a Dissociating Diatomic Gas

Up to this point, both perfect gas and diatomic dissociating gas have been individually evaluated. In this section, we will compare the results of perfect gas HSDT to diatomic dissociating gas HSDT for a power-law shock body. These comparisons are shown in Figs. 4.7 - **??**.

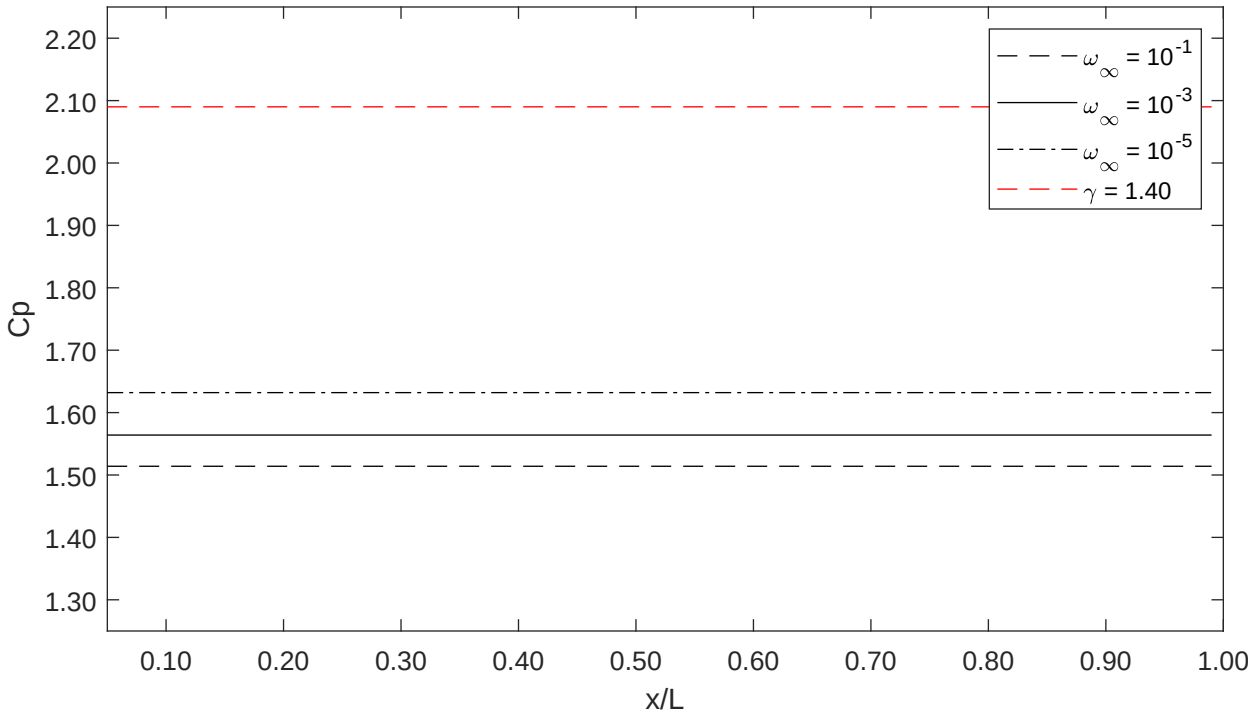

Figure 4.7: Surface Pressure on Power-Law Shock Body Comparison of Perfect to Dissociating Gas (m = 1)

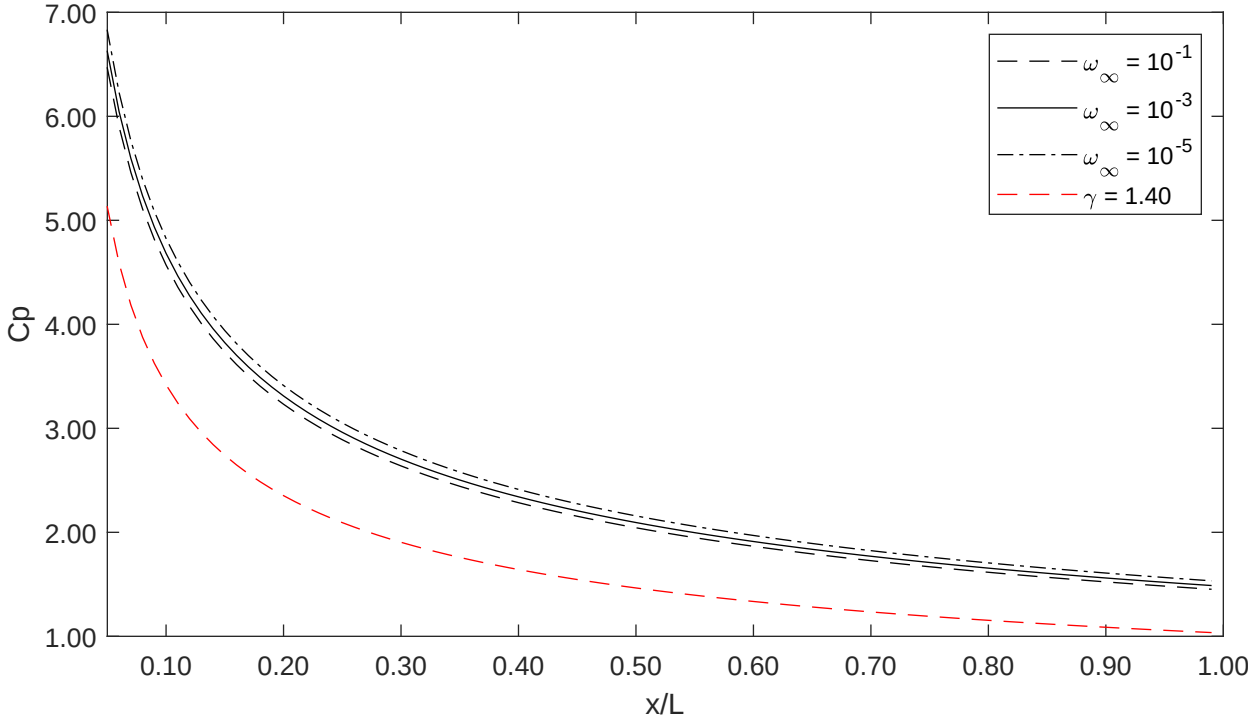

Figure 4.8: Surface Pressure on Power-Law Shock Body Comparison of Perfect to Dissociating Gas (m = 3/4)

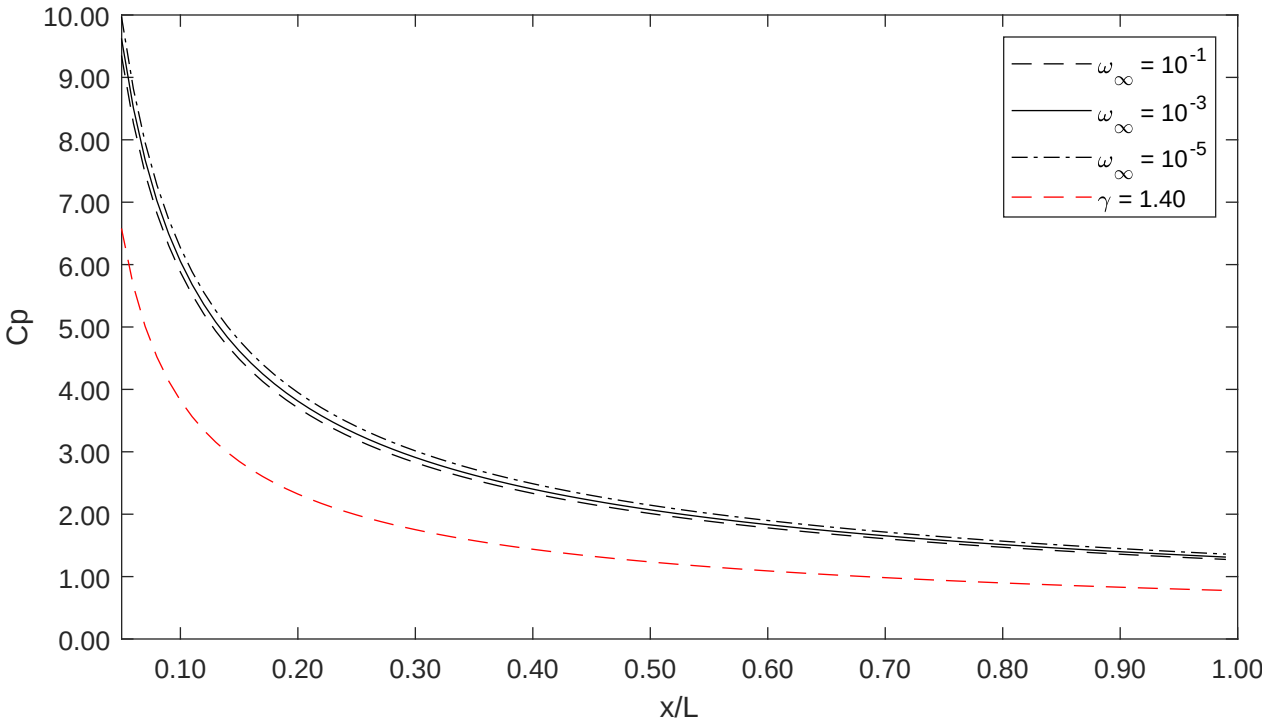

Figure 4.9: Surface Pressure on Power-Law Shock Body Comparison of Perfect to Dissociating Gas (m = 2/3)

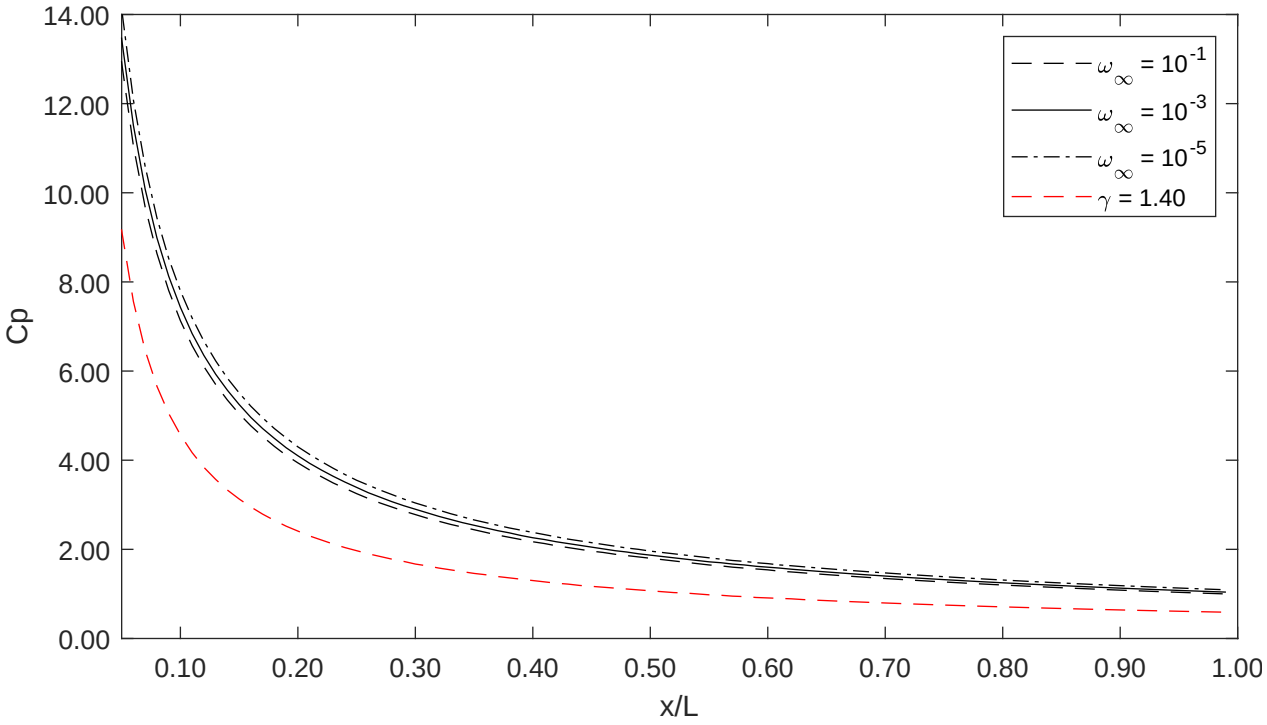

Figure 4.10: Surface Pressure on Power-Law Shock Body Comparison of Perfect to Dissociating Gas (m = 4/7)

From the results, it is observed that the comparison of a perfect gas to a dissociating gas agree qualitatively but there is a non negligible difference. This could most likely be attributed to the dissociations in equilibrium flow.

CHAPTER 5

SUMMARY AND FUTURE WORK

In this study, small disturbance theory is investigated as a method for providing an approximate calculation of a hypersonic flow field. Hypersonic flows on a plane wedge, a circular cone and power-law shock bodies are firstly calculated based on perfect gas approximations. The cone and wedge results agreed well with oblique shock theory. The results are also in agreement with experimental data. Hypersonic flows on power-law shock bodies are then calculated based upon a diatomic dissociating gas approximation. These results agree well with literature and show a qualitative agreement but a non-negligible difference, which could be attributed to dissociations in equilibrium flow. These calculations for perfect gas and diatomic dissociating gas shed some light on the further development of small disturbance theory for more complex hypersonic flows.

During this research, a MATLAB code has been developed to calculate the coefficient of pressure on a circular cone, plane wedge, and slender bodies for perfect gas flow. This code was then expanded to include the calculation of the coefficient of pressure on a slender body in diatomic dissociating gas flow. This code drastically reduces the computational time traditionally required to provide an approximate coefficient of pressure for hypersonic flow. In its current state, this can be used to aid the preliminary/conceptual design of a general hypersonic vehicle but not in the detailed design phase.

Future/follow-on work will include working on self-similar solutions of the inviscid governing equations, equation (2.22), based on a two-temperature internal energy model, five-species air chemistry and/or eleven-species air chemistry. Additional work will include

further development of the MATLAB code to include additional flow variables and flow field visualization plots to aid the preliminary/conceptual design process.

REFERENCES

[1] Milton Van Dyke. A Study of Hypersonic Small-Disturbance Theory. Technical Report TR-1194, NACA, January 1954.

[2] H.S. Tsien. Similarity Laws of Hypersonic Flows. *Journal of Mathematics and Physics*, 25:247–251, 1946.

[3] W.D. Hayes. On Hypersonic Similitude. *Quarterly of Applied Mathematics*, 5:105–106, 1947.

[4] F.M. Hamaker and T.J Wong. The Similarity Law for Nonsteady Hypersonic Flow and Requirements for the Dynamical Similarity of Related Bodies in Free Flight. Technical Report 2631, NACA, 1952.

[5] Milton Van Dyke. Applications of Hypersonic Small-Disturbance Theory. *Journal of the Aeronautical Sciences*, 21:179–186, 1954.

[6] S. Kraus. An Analysis of Supersonic Flow in the Region of the Leading Edge of Curved Airfoils, Including Charts for Determining Surface-Pressure Gradient and Shock-Wave Curvature. Technical Report TN 2729, NACA, 1952.

[7] J.D. Anderson. *Hypersonic and High-Temperature Gas Dynamics*, chapter Hypersonic Inviscid Flowfields: Approximate Methods, pages 103–176. American Institute of Aeronautics and Astronautics, Reston, VA, 2nd edition, 2006.

[8] R.W. Truitt. *Hypersonic Aerodynamics*, chapter Hypersonic Small Disturbance Theory, pages 164–199. The Ronald Press Company, New York, 1st edition, 1959.

[9] M.L. Rasmussen. On hypersonic flow past an unyawed cone. *AIAA Journal*, 5(8):1495–1497, 1967.

[10] R. T. Doty and M. L Rasmussen. Approximation for hypersonic flow past an inclined cone. *AIAA Journal*, 11:1310–1315, 1973.

[11] N. D'Souza and S. Moulder. Applicability of hypersonic small-disturbance theory and similitude to internal hypersonic conical flows. *Journal of Spacecraft and Rockets*, 7(2):149–154, 1970.

[12] Toshi Kubota. *Investigation of Flow Around Simple Bodies in Hypersonic Flow*. PhD thesis, California Institute of Technology, January 1957. CaltechETD: etd-07142004-143403.

[13] J.D. Cole. Newtonian Flow Theory for Slender Bodies. Technical Report RM-1633, RAND Corporation, February 1956.

[14] R.X. Meyer. Hypersonic Flow of a Diatomic Dissociating Gas with Power-Law Shock. Technical report, Aerospace Corporation, El Segundo,CA, November 1968. TR-0200(9990)-3.

[15] M.J. Lighthill. Dynamics of a Dissociating Gas Part 1 Equilibrium flow. *Journal of Fluid Mechanics*, 2(1):1–32, 1957.

[16] X. Wang and X. Zhong. Development and validation of a high-order shock-fitting non-equilibrium flow solver. Technical Report 2011-365, AIAA, January 2011.

[17] C. Park. *Nonequilibrium Hypersonic Aerothermodynamics*. John Wiley and Sons Inc, New York, 1990.

[18] C Mortenson. *Effects of Thermochemical Nonequilibirum on Hypersonic Boundary-Layer Instability in the Presence of Surface Ablation or Isolated Two-Dimensional Roughness*. PhD thesis, University of California, Los Angeles, January 2015.

[19] J.Lee. Basic governing equations for the flight regimes of aeroassisted orbital transfer vehicles. In H.F. Nelson, editor, *Thermal Design of Aeroassisted Orbital Transfer Vehicles*, volume 96, pages 3–53. AIAA, New York, 1985.

[20] R. Millikan and D. White. Systematics of Vibrational Relaxation. *Journal of Chemical Physics*, 39(12):3209–3213, 1963.

[21] Staff of Ames Aeronautical Laboratory. Equations, Tables, and Charts for Compressible Flow. Technical report, Ames Aeronautical Laboratory, May 1953. NACA 1135.

[22] C. Wilke. A Viscosity Equation for Gas Mixtures. *The Journal of Chemical Physics*, 18(4):517–519, 1950.

[23] J.C. Townsend. Second-Order Small-Disturbance Solutions for Hypersonic Flow over Power-Law Bodies. Technical report, NASA, Hampton, VA, 1975. NASA TN D-9793.

[24] J. Lukasiewicz. Hypersonic Flow-Blast Analogy. Technical report, VKF,ARO, Inc., 1961. AEDC-TR-61-4.

APPENDIX A

DERIVATION OF PERFECT GAS EQUATIONS OF MOTION

$$\text{Continuity} \quad \frac{\partial \bar{\rho}}{\partial \bar{x}} + \frac{\partial \bar{\rho}\bar{v}}{\partial \bar{r}} + k\frac{\bar{\rho}\bar{v}}{\bar{r}} = 0 \tag{A.1a}$$

$$\text{R- Momentum} \quad \bar{\rho}\left(\frac{\partial \bar{v}}{\partial \bar{x}} + \bar{v}\frac{\partial \bar{v}}{\partial \bar{r}}\right) + \frac{\partial \bar{p}}{\partial \bar{r}} = 0 \tag{A.1b}$$

$$\text{Energy} \quad \left(\frac{\partial}{\partial \bar{x}} + \bar{v}\frac{\partial}{\partial \bar{r}}\right)\left(\frac{\bar{p}}{\bar{\rho}^{\gamma}}\right) = 0 \tag{A.1c}$$

A.1 Continuity Equation

$$\frac{\partial \bar{\rho}}{\partial \bar{x}} + \frac{\partial \bar{\rho}\bar{v}}{\partial \bar{r}} + k\frac{\bar{\rho}\bar{v}}{\bar{r}} = 0 \tag{A.2}$$

The operator, equation (3.35) is modified to equation (A.3) is applied to the Continuity Equation.

$$\frac{\partial}{\partial \bar{x}} = \frac{\partial}{\partial \bar{x}} + \frac{\bar{R}'}{\bar{R}}(\phi - z)\frac{\partial}{\partial z} - \bar{v}\frac{\partial}{\partial \bar{r}}\,;\ \frac{\partial}{\partial \bar{r}} = \frac{\bar{R}'}{\bar{v}\bar{R}}(\phi - z)\frac{\partial}{\partial z} \tag{A.3}$$

The flow variables, equation (3.34) are substituted into the Continuity Equation.

$$\frac{\partial \bar{\rho}}{\partial \bar{x}} + \frac{\bar{R}'}{\bar{R}}(\phi - z)\frac{\partial \bar{\rho}}{\partial z} - \bar{v}\frac{\partial \bar{\rho}}{\partial \bar{r}} + \frac{\bar{R}'}{\bar{v}\bar{R}}(\phi - z)\frac{\partial \bar{\rho}\bar{v}}{\partial z} + k\frac{\bar{\rho}\bar{v}}{\bar{r}} = 0 \tag{A.4}$$

$$\frac{\partial(\psi(z))}{\partial \bar{x}} + \frac{\bar{R}'}{\bar{R}}(\phi - z)\frac{\partial(\psi(z))}{\partial z} - \bar{R}'(x)\phi(z)\frac{\partial(\psi(z))}{\partial \bar{r}} + \frac{\bar{R}'}{\bar{R}'(x)\phi(z)\bar{R}}(\phi - z)\frac{\partial(\psi(z)\bar{R}'(x)\phi(z))}{\partial z} + k\frac{\psi(z)\bar{R}'(x)\phi(z)}{\bar{r}} = 0 \tag{A.5}$$

$$\frac{\bar{R}'}{\bar{R}}\left(\phi - z\right)\psi'(z) - \frac{\bar{R}'(x)}{\bar{R}(x)}\phi(z)\psi'(z) + \frac{\bar{R}'\bar{R}'(x)}{\bar{R}\prime(x)\phi(z)\bar{R}}\left(\phi - z\right)\left[\psi(z)\phi'(z) + \psi'(z)\phi(z)\right] + k\frac{\psi(z)\bar{R}'(x)\phi(z)}{\bar{R}(x)z} = 0 \quad \text{(A.6)}$$

$$\frac{\bar{R}'}{\bar{R}}[(\phi - z)\psi'(z) - \phi(z)\psi'(z) + \frac{(\phi - z)}{\phi(z)}[\psi(z)\phi'(z) + \psi'(z)\phi(z)] + k\frac{\psi(z)\phi(z)}{z}] = 0 \quad \text{(A.7)}$$

Here $\frac{(\phi - z)}{\phi(z)}$ approaches 1.

$$\frac{\bar{R}'}{\bar{R}}\left[\left(\phi - z\right)\psi'(z) - \phi(z)\psi'(z) + \psi(z)\phi'(z) + \psi'(z)\phi(z) + k\frac{\psi(z)\phi(z)}{z}\right] = 0 \quad \text{(A.8)}$$

$$\frac{\bar{R}'}{\bar{R}}\left[\left(\phi - z\right)\psi'(z) + \psi(z)\phi'(z) + k\frac{\psi(z)\phi(z)}{z}\right] = 0 \quad \text{(A.9)}$$

A.2 Momentum Equation

$$\bar{\rho}\left(\frac{\partial\bar{v}}{\partial\bar{x}} + \bar{v}\,\frac{\partial\bar{v}}{\partial\bar{r}}\right) + \frac{\partial\bar{p}}{\partial\bar{r}} = 0 \quad \text{(A.10)}$$

The operator, equation (3.35) is applied to the Momentum Equation.

$$\bar{\rho}\left(\frac{\partial\bar{v}}{\partial\bar{x}} + \frac{\bar{R}'}{\bar{R}}\left(\phi - z\right)\frac{\partial\bar{v}}{\partial z}\right) + \frac{\partial\bar{p}}{\partial\bar{r}} = 0 \quad \text{(A.11)}$$

The flow variables, equation(3.34) are substituted into the Momentum Equation.

$$\psi\left(z\right)\left(\frac{\partial\left(\bar{R}'(x)\phi(z)\right)}{\partial\bar{x}} + \frac{\bar{R}'}{\bar{R}}\left(\phi - z\right)\frac{\partial\left(\bar{R}'(x)\phi(z)\right)}{\partial z}\right) + \frac{\partial\left(\bar{R}'^{2}(x)F(z)\right)}{\partial\bar{r}} = 0 \quad \text{(A.12)}$$

$$\psi\left(z\right)\bar{R}''(x)\phi(z) + \frac{\bar{R}'}{\bar{R}}\left(\phi - z\right)\bar{R}'(x)\phi'(z)\psi(z) + \frac{\bar{R}'^{2}(x)F'(z)}{\bar{R}} = 0 \quad \text{(A.13)}$$

$$\psi(z)\,\bar{R}''(x)\phi(z) + \frac{\bar{R}'^2}{\bar{R}}(\phi - z)\,\phi'(z)\psi(z) + \frac{\bar{R}'^2(x)F'(z)}{\bar{R}} = 0 \tag{A.14}$$

$$\bar{R}''(x)\phi(z) + \frac{\bar{R}'^2}{\bar{R}}(\phi - z)\,\phi'(z) + \frac{\bar{R}'^2(x)F'(z)}{\bar{R}\,\psi(z)} = 0 \tag{A.15}$$

$$\frac{\bar{R}''(x)\bar{R}^2}{\bar{R}'}\,\phi(z) + (\phi - z)\,\phi'(z) + \frac{F'(z)}{\psi(z)} = 0 \tag{A.16}$$

A.3 Energy Equation

$$\left(\frac{\partial}{\partial\bar{x}} + \bar{v}\frac{\partial}{\partial\bar{r}}\right)\left(\frac{\bar{p}}{\bar{\rho}^\gamma}\right) = 0 \tag{A.17}$$

The operator, equation (3.35) is applied to the Energy Equation.

$$\left(\frac{\partial}{\partial\bar{x}} + \frac{\bar{R}'}{\bar{R}}(\phi - z)\frac{\partial}{\partial z}\right)\left(\frac{\bar{p}}{\bar{\rho}^\gamma}\right) = 0 \tag{A.18}$$

The flow variables, equation(3.34) are substituted into the Energy Equation.

$$\left(\frac{\partial}{\partial\bar{x}} + \frac{\bar{R}'}{\bar{R}}(\phi - z)\frac{\partial}{\partial z}\right)\left(\frac{\bar{R}'^2(x)F(z)}{\psi(z)^\gamma}\right) = 0 \tag{A.19}$$

$$\left(\frac{2\bar{R}''\bar{R}'(x)F(z)}{\psi(z)^\gamma} + \frac{\bar{R}'}{\bar{R}}(\phi - z)\frac{\bar{R}'^2(x)F(z)}{\psi(z)^\gamma}\frac{\partial}{\partial z}\right) = 0 \tag{A.20}$$

$$\left(\frac{2\bar{R}''\bar{R}'(x)F(z)}{\psi(z)^\gamma} + \frac{\bar{R}'\bar{R}'^2(x)}{\bar{R}}(\phi - z)\left[\frac{\psi(z)^\gamma F'(z) - F(z)\gamma\psi(z)^{\gamma-1}\psi'(z)}{(\psi(z)^\gamma)^2}\right]\right) = 0 \tag{A.21}$$

$$\frac{2\bar{R}''\bar{R}}{\bar{R}'^2} + (\phi - z)\frac{\psi(z)^\gamma}{F(z)}\left[\frac{\psi(z)^\gamma F'(z) - F(z)\gamma\psi(z)^{\gamma-1}\psi'(z)}{(\psi(z)^\gamma)^2}\right] = 0 \tag{A.22}$$

$$\frac{2\bar{R}''\bar{R}}{\bar{R}'^2} + (\phi - z)\left[\frac{(\psi(z)^\gamma)^2 F'(z)}{(\psi(z)^\gamma)^2 F(z)} - \frac{F(z)\ \gamma\ \psi(z)^\gamma\ \psi(z)^{\gamma-1}\ \psi'(z)}{(\psi(z)^\gamma)^2 F(z)}\right] = 0 \tag{A.23}$$

$$\frac{2\bar{R}''\bar{R}}{\bar{R}'^2} + (\phi - z)\left[\frac{F'(z)}{F(z)} - \frac{\gamma\ \ \psi(z)^{\gamma-1}\ \psi'(z)}{\psi(z)^\gamma}\right] = 0 \tag{A.24}$$

$$\frac{2\bar{R}''\bar{R}}{\bar{R}'^2} + \ (\phi - z)\left[\frac{F'(z)}{F(z)} \ - \gamma\frac{\psi'(z)}{\psi(z)}\right] = 0 \tag{A.25}$$

APPENDIX B

DERIVATION OF DISSOCIATING GAS EQUATIONS OF MOTION

$$\text{Continuity} \quad \frac{\partial \bar{\omega}}{\partial x} + \frac{\partial \bar{\omega}\bar{v}}{\partial y} + j\frac{\bar{\omega}\bar{v}}{y} = 0 \tag{B.1a}$$

$$\text{Momentum} \quad \left(\frac{\partial}{\partial x} + \bar{v}\frac{\partial}{\partial y}\right)\bar{v} + \frac{1}{\bar{\omega}}\frac{\partial \bar{p}}{\partial y} = 0 \tag{B.1b}$$

$$\text{Energy} \quad \left(\frac{\partial}{\partial x} + \bar{v}\frac{\partial}{\partial y}\right)\bar{s} = 0 \tag{B.1c}$$

B.1 Continuity Equation

$$\frac{\partial \bar{\omega}}{\partial x} + \frac{\partial \bar{\omega}\bar{v}}{\partial y} + j\frac{\bar{\omega}\bar{v}}{y} = 0 \tag{B.2}$$

The operator, equation (4.2) is applied to the Continuity Equation.

$$\frac{\partial \bar{\omega}}{\partial \xi} - \frac{m\eta}{\xi}\frac{\partial \bar{\omega}}{\partial \eta} + \frac{m}{\xi^m}\frac{\partial \bar{\omega}\bar{v}}{\partial \eta} + j\frac{\bar{\omega}\bar{v}}{y} = 0 \tag{B.3}$$

The functions, f_1 and f_5, equation (4.3), and y are substituted into the equation.

$$\frac{\partial\left(\frac{1}{f_5(\eta)}\right)}{\partial \xi} - \frac{m\eta}{\xi}\frac{\partial\left(\frac{1}{f_5(\eta)}\right)}{\partial \eta} + \frac{m}{\xi^m}\frac{\partial\left(\frac{1}{f_5(\eta)}\xi^{m-1}f_1(\eta)\right)}{\partial \eta} + j\frac{\left(\frac{1}{f_5(\eta)}\right)\xi^{m-1}f_1(\eta)}{\frac{\eta\xi^m}{m}} = 0 \tag{B.4}$$

$$\frac{m\eta}{\xi}\frac{f_5'(\eta)}{f_5(\eta)^2} + \frac{m\xi^{m-1}}{\xi^m}\left[\frac{f_1'(\eta)}{f_5(\eta)} - \frac{f_1(\eta)f_5'(\eta)}{f_5(\eta)^2}\right] + \frac{j}{\eta}\frac{m\left(\frac{1}{f_5(\eta)}\right)\xi^{m-1}f_1(\eta)}{\xi^m} = 0 \tag{B.5}$$

$$\frac{\eta}{\xi}\frac{f_5'(\eta)}{f_5(\eta)^2}+\frac{\xi^{m-1}}{\xi^m}\left[\frac{f_1'(\eta)}{f_5(\eta)}-\frac{f_1(\eta)f_5'(\eta)}{f_5(\eta)^2}\right]+\frac{j}{\eta}\frac{\left(\frac{1}{f_5(\eta)}\right)\xi^{m-1}f_1(\eta)}{\xi^m} = 0 \tag{B.6}$$

$$\frac{\eta}{\xi}\frac{f_5'(\eta)}{f_5(\eta)^2}+\frac{1}{\xi}\left[\frac{f_1'(\eta)}{f_5(\eta)}-\frac{f_1(\eta)f_5'(\eta)}{f_5(\eta)^2}\right]+\frac{j}{\eta}\frac{\left(\frac{1}{f_5(\eta)}\right)f_1(\eta)}{\xi} = 0 \tag{B.7}$$

$$\eta\frac{f_5'(\eta)}{f_5(\eta)^2}+\frac{f_1'(\eta)}{f_5(\eta)}-\frac{f_1(\eta)f_5'(\eta)}{f_5(\eta)^2}+\frac{j}{\eta}\left(\frac{1}{f_5(\eta)}\right)f_1(\eta) = 0 \tag{B.8}$$

$$\eta f_5'(\eta)+f_1'(\eta)f_5(\eta)-f_1(\eta)f_5'(\eta)+\frac{j}{\eta}f_5(\eta)f_1(\eta) = 0 \tag{B.9}$$

$$f_5'(\eta)(\eta-f_1(\eta))+f_1'(\eta)f_5(\eta)+\frac{j}{\eta}f_5(\eta)f_1(\eta) = 0 \tag{B.10}$$

B.2 Momentum Equation

$$\left(\frac{\partial}{\partial x}+\bar{v}\frac{\partial}{\partial y}\right)\bar{v}+\frac{1}{\bar{\omega}}\frac{\partial\bar{p}}{\partial y} = 0 \tag{B.11}$$

The operator, equation (4.2) is applied to Momentum Equation.

$$\left(\frac{\partial}{\partial\xi}-\frac{m\eta}{\xi}\frac{\partial}{\partial\eta}+\bar{v}\frac{m}{\xi^m}\frac{\partial}{\partial\eta}\right)\bar{v}+\frac{1}{\bar{\omega}}\frac{m}{\xi^m}\frac{\partial\bar{p}}{\partial\eta} = 0 \tag{B.12}$$

The functions, f_1 ,f_2 and f_5, equation (4.3), are substituted into the equation.

$$\left(\frac{\partial\left(\xi^{m-1}f_1(\eta)\right)}{\partial\xi}-\frac{m\eta}{\xi}\frac{\partial\left(\xi^{m-1}f_1(\eta)\right)}{\partial\eta}+\bar{v}\frac{m}{\xi^m}\frac{\partial\left(\xi^{m-1}f_1(\eta)\right)}{\partial\eta}\right) + \frac{mf_5(\eta)}{\xi^m}\frac{\partial\left(\xi^{2(m-1)}f_2(\eta)\right)}{\partial\eta} = 0 \tag{B.13}$$

$$(m-1)\xi^{m-2}f_1(\eta)-\frac{m\eta\xi^{m-1}}{\xi}f_1'(\eta)+\bar{v}\frac{m\xi^{m-1}}{\xi^m}f_1'(\eta)+\frac{m\xi^{2(m-1)}f_5(\eta)}{\xi^m}f_2'(\eta) = 0 \tag{B.14}$$

$$\frac{(m-1)}{\xi}f_1(\eta)-\frac{m\eta}{\xi}f_1'(\eta)+\bar{v}\frac{m}{\xi^m}f_1'(\eta)+\frac{m\xi^{m-1}}{\xi^m}f_5(\eta)f_2'(\eta) = 0 \tag{B.15}$$

$$\frac{(m-1)}{\xi}f_1(\eta)-\frac{m\eta}{\xi}f_1'(\eta)+\xi^{m-1}f_1(\eta)\frac{m}{\xi^m}f_1'(\eta)+\frac{m\xi^{m-1}}{\xi^m}f_5(\eta)f_2'(\eta) = 0 \tag{B.16}$$

$$(m-1)\,f_1(\eta) - m\eta f_1'(\eta) + m f_1'(\eta) f_1(\eta) + m f_5(\eta) f_2'(\eta) \;=\; 0 \tag{B.17}$$

$$(m-1)\,f_1(\eta) - m\,(\eta - f_1(\eta))\,f_1'(\eta) + m f_5(\eta) f_2'(\eta) \;=\; 0 \tag{B.18}$$

B.3 Energy Equation

$$\left(\frac{\partial}{\partial x} \;+\; \bar{v}\frac{\partial}{\partial y}\right)\bar{s} = \; 0 \tag{B.19}$$

The operator, equation (4.2) is applied to Energy Equation.

$$\left(\frac{\partial}{\partial \xi} - \frac{m\eta}{\xi}\frac{\partial}{\partial \eta} + \bar{v}\frac{m}{\xi^m}\frac{\partial}{\partial \eta}\right)\bar{s} = \; 0 \tag{B.20}$$

The variable, $\bar{s}$ can be defined from f_2 and f_3 as shown in equation, (B.21).

$$\bar{s} \;=\; \xi^{2(m-1)} f_2(\eta) f_3(\eta) \tag{B.21}$$

Equation (B.21) is then applied to the Energy Equation.

$$\frac{\partial(\xi^{2(m-1)} f_2(\eta) f_3(\eta))}{\partial \xi} - \frac{m\eta}{\xi}\frac{\partial(\xi^{2(m-1)} f_2(\eta) f_3(\eta))}{\partial \eta} + \bar{v}\frac{m}{\xi^m}\frac{\partial(\xi^{2(m-1)} f_2(\eta) f_3(\eta))}{\partial \eta} = \; 0 \tag{B.22}$$

$$2(m-1)\xi^{2m-3} f_2(\eta) f_3(\eta)) - \frac{m\eta\xi^{2(m-1)}}{\xi}(f_2(\eta) f_3(\eta))' + \bar{v}\frac{m\xi^{2(m-1)}}{\xi^m}(f_2(\eta) f_3(\eta))' = \; 0 \tag{B.23}$$

$$\frac{2(m-1)}{\xi} f_2(\eta) f_3(\eta)) - \frac{m\eta}{\xi}(f_2(\eta) f_3(\eta))' + \frac{m\xi^{m-1} f_1(\eta)}{\xi^m}(f_2(\eta) f_3(\eta))' = \; 0 \tag{B.24}$$

$$\frac{2(m-1)}{\xi} f_2(\eta) f_3(\eta)) - \frac{m\eta}{\xi}(f_2(\eta) f_3(\eta))' + \frac{m f_1(\eta)}{\xi}(f_2(\eta) f_3(\eta))' = \; 0 \tag{B.25}$$

$$2(m-1) f_2(\eta) f_3(\eta)) - m\eta(f_2(\eta) f_3(\eta))' + m f_1(\eta)(f_2(\eta) f_3(\eta))' = \; 0 \tag{B.26}$$

$$2(m-1) f_2(\eta) f_3(\eta)) - m(\eta - f_1(\eta))(f_2(\eta) f_3(\eta))' = \; 0 \tag{B.27}$$

APPENDIX C

CONVERSION OF GOVERNING EQUATIONS TO MATLAB CODE

C.1 Perfect Gas over Power-Law Shock Body

The governing equations for perfect gas flow over a power-law shock body, equation (C.1) can be coupled together to solve the ordinary differential equations.

$$(\phi - z)\,\psi' + \psi\phi' + k\frac{\psi\phi}{z} = 0 \tag{C.1a}$$

$$(\phi - z)\,\psi' + \frac{F'}{\psi} - \left(\frac{1}{m} - 1\right)\phi = 0 \tag{C.1b}$$

$$(\phi - z)\,\psi'\left[\frac{F'}{F} - \gamma\left(\frac{\psi'}{\psi}\right)\right] - 2\left(\frac{1}{m} - 1\right) = 0 \tag{C.1c}$$

The Continuity Equation, equation (C.1a), is rewritten in terms of ψ' and is shown in equation, (C.2).

$$\psi' = \frac{-k\dfrac{\phi\psi}{z} - \psi\phi'}{\phi - z} \tag{C.2}$$

The Momentum Equation, equation (C.1c), is rewritten in terms of F' and is shown in equation, (C.3)

$$\phi' = \frac{(\dfrac{1}{m} - 1)\phi - \dfrac{F'}{\psi}}{\phi - z} \tag{C.3}$$

The Energy Equation, equation (C.1c), is rewritten in terms of F' and is shown in equation, (C.4)

$$F' = F\left[\frac{2(\frac{1}{m}-1)}{\phi - z} + \gamma\left(\frac{\psi'}{\psi}\right)\right] \tag{C.4}$$

ϕ' is then substituted into ψ'.

$$\psi' = \frac{-k\frac{\psi\phi}{z} - \psi\frac{(\frac{1}{m}-1)\psi\phi - \frac{F'}{\psi}}{\phi - z}}{\phi - z} \tag{C.5}$$

$$\psi' = \frac{-k\frac{\psi\phi}{z} - \frac{(\frac{1}{m}-1)\psi\phi - F'}{\phi - z}}{\phi - z} \tag{C.6}$$

$$\psi' = \frac{-k\frac{\psi\phi}{z}}{\phi - z} - (\frac{1}{m}-1)\psi\phi - F \tag{C.7}$$

$$\psi' = \frac{-k\frac{\psi\phi}{z}}{\phi - z} - (\frac{1}{m}-1)\psi\phi - F\left[\frac{2(\frac{1}{m}-1)}{\phi - z} + \gamma\left(\frac{\psi'}{\psi}\right)\right] \tag{C.8}$$

$$\psi' = \frac{-k\frac{\psi\phi}{z}}{\phi - z} - (\frac{1}{m}-1)\psi\phi - F\frac{2(\frac{1}{m}-1)}{\phi - z} - F\gamma\left(\frac{\psi'}{\psi}\right) \tag{C.9}$$

$$\psi' + F\gamma\left(\frac{\psi'}{\psi}\right) = \frac{-k\frac{\psi\phi}{z}}{\phi - z} - (\frac{1}{m}-1)\psi\phi - F\frac{2(\frac{1}{m}-1)}{\phi - z} \tag{C.10}$$

$$\psi'(1 + \frac{F\gamma}{\psi}) = \frac{-k\frac{\psi\phi}{z}}{\phi - z} - (\frac{1}{m}-1)\psi\phi - F\frac{2(\frac{1}{m}-1)}{\phi - z} \tag{C.11}$$

$$\psi' = \frac{\frac{-k\frac{\psi\phi}{z}}{\phi - z} - (\frac{1}{m}-1)\psi\phi - F\frac{2(\frac{1}{m}-1)}{\phi - z}}{(1 + \frac{F\gamma}{\psi})} \tag{C.12}$$

ψ' is then substituted into F'

$$F' = F\left[\frac{2(\frac{1}{m}-1)}{\phi - z} + \gamma\left(\frac{\frac{-k\frac{\psi\phi}{z}}{\phi - z} - (\frac{1}{m}-1)\psi\phi - F\frac{2(\frac{1}{m}-1)}{\phi - z}}{(\phi - z)(1+\frac{F\gamma}{\psi})\ \psi}\right)\right] \tag{C.13}$$

F' is then substituted into ϕ'

$$\phi' = \frac{(\frac{1}{m}-1)\phi\ -\ \dfrac{F\left[\dfrac{2(\frac{1}{m}-1)}{\phi - z} + \gamma\left(\dfrac{\dfrac{-k\frac{\psi\phi}{z}}{\phi - z} - (\frac{1}{m}-1)\psi\phi - F\frac{2(\frac{1}{m}-1)}{\phi - z}}{(\phi - z)(1+\frac{F\gamma}{\psi})\ \psi}\right)\right]}{\psi}}{\phi - z} \tag{C.14}$$

C.2 Diatomic Dissociating Gas over Power-Law Shock Body

The governing equations for diatomic dissociating gas flow over a power-law shock body, equation (C.15) can be coupled together to solve the ordinary differential equations.

$$f_1' f_5 + (\eta - 1)\, f_5' + \left(\frac{j}{\eta}\right) f_1 f_5 = 0 \tag{C.15a}$$

$$(m-1)\, f_1 - m\,(\eta - f_1)\, f_1' + m f_2' f_5 = 0 \tag{C.15b}$$

$$2\,(m-1)\, f_2 f_3 - m\,(\eta - f_1)\,(f_2 f_3)' = 0 \tag{C.15c}$$

$$f_4 - \omega_\infty \phi\left(\omega_\infty^{-1} f_3\right) = 0 \tag{C.15d}$$

$$f_5 - \omega_\infty \chi\left(\omega_\infty^{-1} f_3\right) = 0 \tag{C.15e}$$

The values of f_1', f_2', f_3' and f_5' are found in sections C.2.1 - C.2.4.

C.2.1 f_1'

$$f_5 f_1' \ + \ 0 f_2' + (\eta - 1)(\frac{f_5}{f_3})(\frac{d \ln \chi}{d \ln z/p}) f_3' = \ -(\frac{j}{\eta}) f_1 f_5 \tag{C.16}$$

$$f_5 f_1' \ = \ -(\frac{j}{\eta}) f_1 f_5 - (\eta - 1)(\frac{f_5}{f_3})(\frac{d \ln \chi}{d \ln z/p}) f_3' \tag{C.17}$$

$$f_1' \ = \ \frac{-(\frac{j}{\eta}) f_1 f_5 - (\eta - 1)(\frac{f_5}{f_3})(\frac{d \ln \chi}{d \ln z/p}) f_3'}{f_5} \tag{C.18}$$

$$f_1' \ = \ -(\frac{j}{\eta}) f_1 - (\eta - 1)(\frac{1}{f_3})(\frac{d \ln \chi}{d \ln z/p}) f_3' \tag{C.19}$$

C.2.2 f_2'

$$a_{21} f_1' \ + \ m f_5 f_2' + 0 f_3' = \ -(m - 1) f_1 \tag{C.20}$$

Where $a_{21} = -m(\eta - f_1)$.

$$m f_5 f_2' = \ -(m - 1) f_1 - a_{21} f_1' \tag{C.21}$$

$$f_{2\prime} = \ \frac{-(m - 1) f_1 - a_{21} f_{1\prime}}{m f_5} \tag{C.22}$$

C.2.3 f_3'

$$a_{21} f_3 f_2' + \ a_{21} f_2 f_{3\prime} = \ -2(m - 1) f_2 f_3 \tag{C.23}$$

$$a_{21} f_3 \left[\frac{-(m - 1) f_1 - a_{21} f_1'}{m f_5} \right] \ + \ a_{21} f_2 f_3' = \ -2(m - 1) f_2 f_3 \tag{C.24}$$

$$-(m - 1) a_{21} f_1 f_3 - a_{21}^2 f_3 f_1' + \ m a_{21} f_2 f_5 f_3' = \ -2(m - 1) f_2 f_3 m \tag{C.25}$$

$$-a_{21}^2 f_3 f_1' + \ m a_{21} f_2 f_5 f_3' = \ -2(m - 1) f_2 f_3 m + (m - 1) a_{21} f_1 f_3 \tag{C.26}$$

$$- a_{21}^2 f_3 \left[-(\frac{j}{\eta}) f_1 - (\eta - 1)(\frac{1}{f_3})(\frac{d \ln \chi}{d \ln z/p}) f_3' \right] + \ m a_{21} f_2 f_5 f_3' =$$

$$- 2(m-1) f_2 f_3 m + (m-1) a_{21} f_1 f_3 \quad \text{(C.27)}$$

$$a_{21}^2 f_3 (\frac{j}{\eta}) f_1 + a_{21}^2 (\eta - 1)(\frac{d \ln \chi}{d \ln z/p}) f_3' + \ m a_{21} f_2 f_5 f_3' =$$

$$- 2(m-1) f_2 f_3 m + (m-1) a_{21} f_1 f_3 \quad \text{(C.28)}$$

$$a_{21}^2 (\eta - 1)(\frac{d \ln \chi}{d \ln z/p}) f_3' + m a_{21} f_2 f_5 f_3' =$$

$$- 2(m-1) f_2 f_3 m + (m-1) a_{21} f_1 f_3 - a_{21}^2 f_3 (\frac{j}{\eta}) f_1 \quad \text{(C.29)}$$

$$f_3' = \frac{-2(m-1) f_2 f_3 m + (m-1) a_{21} f_1 f_3 - a_{21}^2 f_3 (\frac{j}{\eta}) f_1}{a_{21}^2 (\eta - 1)(\frac{d \ln \chi}{d \ln z/p}) + \ m a_{21} f_2 f_5} \quad \text{(C.30)}$$

C.2.4 f_5'

$$f_5' = (\frac{f_5}{f_3})(\frac{d \ln \chi}{d \ln z/p}) f_3' \quad \text{(C.31)}$$

APPENDIX D

MATLAB CODE - PERFECT GAS AND DIATOMIC DISSOCIATING GAS

Below is the MATLAB Code that was developed for the calculation of the coefficient of pressure for a perfect gas and diatomic dissociating gas shown in Chapter 3 and Chapter 4, respectively. This code was developed in the academic version of MATLAB R2018b. It should be noted that the ode45 function used in this code was developed by Mark W. Reichelt and Lawrence R. Shampine for The Mathworks, Inc. and can be found in MATLAB R2018b.

```
function [perfect,dissociating] = HSDT(m,L,k,gamma,omegainf)
%% ..........................................................%%
%% Created by: Andrew Wuetcher, University of Alabama, October 2018
%
%% Variable Definition
% L = Length of Power-Law Shock Body
% m = exponent, rb~ x^m (1/2; 4/7; 2/3; 3/4)
% k = defines plane or axisymmetric flow
% gamma = specific heat ratio
% omegainf = density
% halt = altitude
% Mach = Freestream Mach Condition

%% Values not valid for the nose region
%%..........................................................%%
%% Global Definitions
format long;
x(:,1) = 0:0.01:L;
y(:,1) = (x.^m)./m;
zeta(:,1) = x;
```

```
rb = x.^m;
delta = (rb./L)./(x./L).^m;

for i = 1:length(x)
    if i == length(x)
        anglesigma(i,1) = cos((x(i,1)-x(i-1,1))/(y(i,1)-y(i-1,1)));
    else
        anglesigma(i,1) = cos((x(i+1,1)-x(i+1,1))/(y(i+1,1)-y(i,1))) ;
    end
end
%% Perfect Gas
% Boundary Conditions at Shock
%         Psi(1)              Phi(1)              F(1)
bc = [((gamma+1)/(gamma-1)) (2/(gamma+1)) (2/(gamma+1)) ];
zspan = 1:-0.0001:0;

% ODE45 Solver
% y(1) Psi
% y(2) F
% y(3) Phi

F = @(z,y) [((-y(1)*(((2*((1/m)-1)*y(2))-((gamma*k*y(3)*y(2))/z)-((y(3)-z)*y(1)*y(3)*((1/m)
    -1)))/((gamma*y(2))-(y(1)*((y(3)-z)^2)))))-(k*((y(1)*y(3))/z)))/(y(3)-z))
            ((y(1)*((1/m)-1)*y(3))-(y(1)*(y(3)-z)*(((2*((1/m)-1)*y(2))-((gamma*k*y(3)*y(2))/
                z)-((y(3)-z)*y(1)*y(3)*((1/m)-1)))/((gamma*y(2))-(y(1)*((y(3)-z)^2))))));
            (((2*((1/m)-1)*y(2))-((gamma*k*y(3)*y(2))/z)-((y(3)-z)*y(1)*y(3)*((1/m)-1)))/((
                gamma*y(2))-(y(1)*((y(3)-z)^2))))];
 Opt     = odeset('Events', @myEvent);

[z,y] = ode45(F,zspan,bc,Opt);
y(any(isnan(y),2),:) = [];
l = length(y(:,2));
perfect.z = z;
perfect.y = y;
perfect.x(:,1) = x./L;
perfect.Cp(:,1) =( 2*y(end,2)/(z(l,1)^2))*(m^2)*(delta.^2).*((x/L).^(2*(m-1)));

%% Dissociating Gas
% Boundary Conditions at Shock
% Find value of alpha corresponding to appropriate density
for alpha = 0:0.0000001:1
```

```
59      a = omegainf*(((alpha^2)/(1-alpha))*exp((5-2*alpha-(alpha^2))/(1-alpha)))*(5+2*alpha
            +(2/(1-alpha)));
60      if a >= 1
61          alpha = alpha;
62          break;
63      end
64  end
65
66  f5 = omegainf*(((alpha^2)/(1-alpha))*exp((5-2*alpha-(alpha^2))/(1-alpha)));
67  f4 = omegainf*(((alpha^2)/(1-alpha))*exp((5-2*alpha-(alpha^2))/(1-alpha)))*(3+alpha+(1/(1-
        alpha)));
68  chi = f5/omegainf;
69  lnchi = log(chi);
70
71  p1 =    7.225e-06;
72  p2 =   -0.0002965;
73  p3 =    -0.002451;
74  p4 =        1.359;
75  p5 =       0.3933;
76
77  lnzpchi = p1*lnchi^4 + p2*lnchi^3 + p3*lnchi^2 + p4*lnchi + p5;
78
79  f1 = 1-f5;
80  f2 = f1;
81  zp = exp(lnzpchi);
82  f3 = zp*omegainf;
83
84  bc = [f1  f2  f3  f5];
85
86  upperlnchi = lnchi+0.01;
87  lowerlnchi = lnchi-0.01;
88  dlnchi = upperlnchi-lowerlnchi;
89  upperlnzp = p1*upperlnchi^4 + p2*upperlnchi^3 + p3*upperlnchi^2 + p4*upperlnchi + p5;
90  lowerlnzp = p1*lowerlnchi^4 + p2*lowerlnchi^3 + p3*lowerlnchi^2 + p4*lowerlnchi + p5;
91  dlnzp = upperlnzp-lowerlnzp;
92  dlnchidlnzp = dlnchi/dlnzp;
93
94  % ODE45 solver
95  % y(1)  f1
96  % y(2)  f2
97  % y(3)  f3
```

```
98  % y(4) f5
99
100 F = @(q,f)[(-(k/q)*f(1)-(q-f(1))*(1/f(3))*dlnchidlnzp*(((-2*(m-1)*f(2)*f(3)*f(4)*m)+(-m*(q-f
        (1))*f(1)*f(3)*(m-1))-(((-m*(q-f(1)))^2)*f(1)*f(3)*(k/q)))/((((-m*(q-f(1)))^2)*(q-f(1))*
        dlnchidlnzp)+(-m*(q-f(1))*f(2)*f(4)*m))));...
101             ((-(m-1)*f(1)-(-m*(q-f(1)))*(-(k/q)*f(1)-(q-f(1))*(1/f(3))*dlnchidlnzp*(((-2*(m
                    -1)*f(2)*f(3)*f(4)*m)+(-m*(q-f(1))*f(1)*f(3)*(m-1))-(((-m*(q-f(1)))^2)*f(1)*f
                    (3)*(k/q)))/((((-m*(q-f(1)))^2)*(q-f(1))*dlnchidlnzp)+(-m*(q-f(1))*f(2)*f(4)*
                    m)))))/(m*f(4)));  ...
102             (((-2*(m-1)*f(2)*f(3)*f(4)*m)+(-m*(q-f(1))*f(1)*f(3)*(m-1))-(((-m*(q-f(1)))^2)*f
                    (1)*f(3)*(k/q)))/((((-m*(q-f(1)))^2)*(q-f(1))*dlnchidlnzp)+(-m*(q-f(1))*f(2)*
                    f(4)*m)));...
103             (f(4)/f(3))*dlnchidlnzp*(((-2*(m-1)*f(2)*f(3)*f(4)*m)+(-m*(q-f(1))*f(1)*f(3)*(m
                    -1))-(((-m*(q-f(1)))^2)*f(1)*f(3)*(k/q)))/((((-m*(q-f(1)))^2)*(q-f(1))*
                    dlnchidlnzp)+(-m*(q-f(1))*f(2)*f(4)*m)))];
104
105 qspan = 1:-0.0001:0;
106 Opt   = odeset('Events', @myEventdis);
107 [q,y] = ode45(F,qspan,bc,Opt);
108 y(any(isnan(y),2),:) = [];
109
110 meyer.f1 = y(:,1);
111 meyer.f2 = y(:,2);
112 meyer.f3 = y(:,3);
113 meyer.f5 = y(:,4);
114 meyer.q  = q(:,1);
115
116 meyer.Cp = 2.*(anglesigma(:,1).^2).*(zeta(:,1).^(2.*(m-1))).*meyer.f2(end,1);
117
118 %% Plot of Dissociating Gas vs. Perfect Gas
119 plot(x(:,1),meyer.Cp,x(:,1),perfect.Cp);
120 axis([ 0.05 1 0 20]);
121 xlabel('x/L');
122 ylabel('Cp');
123 legend('Dissociating Gas','Perfect Gas')
124 end
125
126 function [value, isterminal, direction] = myEvent(z,y)
127 value      = (y(3) >= z);
128 isterminal = 1;
129 direction  = 0;
```

```
130 end
131
132 function [value, isterminal, direction] = myEventdis(q,y)
133 value      = (y(2) >= q);
134 isterminal = 1;
135 direction  = 1;
136 end
```